Acta Geochim (2025) 44:880–911
https://doi.org/10.1007/s11631-025-00771-0

ORIGINAL ARTICLE

Petrographic and geochemical perspectives on sandstones of the extra-peninsular Gondwana Group from the Arunachal Himalayas, NE India: Probing provenance, tectonic context and paleoenvironmental conditions

Yadav Krishna Gogoi[1,2] · Pradip Borgohain[1] · Diganta Bhuyan[2] · Devojit Bezbaruah[2] · Garima Konwar[1] · Manash Pratim Gogoi[1] · Bubul Bharali[3]

Received: 22 August 2024 / Revised: 25 February 2025 / Accepted: 26 February 2025 / Published online: 2 April 2025

Abstract The extra-peninsular Gondwana Group rocks are exposed in narrow patches within the Lesser Himalayan sequence of the NE-Arunachal Himalayas, India. The bulk of sediments for the sandstones of the Gondwana Group were derived from felsic/acidic to intermediate igneous rocks, with minor mafic input from the upper continental crust (UCC), as supported by various discrimination diagrams based on quantification of detrital minerals coupled with sandstone geochemistry. The inputs from metamorphic sources in subordinate amounts cannot be ruled out, as indicated by quantification of the quartz varieties. These sediments were found to be sourced from the interior part of a craton or shield and recycled platformal sediments which were derived from both passive and active margin settings. The sediments experienced a wide variance in climatic conditions, from arid to humid, suffering low–moderate-intensity weathering (CIA: 63.43; CIW: 86.18; WIP: 44.84; PIA: 75.37; ICV: 2.39; *C*-value: 0.42; PF: 0.49; Sr/Cu: 9.23 and Rb/Sr: 1.68) within the vicinity of the low plains to moderate hills. Additionally, redox-sensitive elements indicate the deposition of sediments under oxygenated or oxygen-rich conditions (U_{au}: −2.91; Th/U: 7.37; U/Th: 0.18; V/Cr: 1.71; δU: 0.67 and Ce/Ce*: 0.93).

Keywords Gondwana Group · Arunachal Himalayas · Provenance and tectonic setting · Paleoclimate · Paleoweathering

1 Introduction

Since their inception, the petrography and geochemistry of rocks and sediments have been used as preeminent proxies to decipher sediment sources, tectonic settings, sediment weathering trends, and paleoconditions, including paleoclimate and paleoredox. Geochemical aspects including major oxide, trace element, and rare earth element (REE) analysis, as well as petrographic approaches for clastic sedimentary rocks, are indispensable tools for reconstructing provenance (Shaw 1968; Basu et al. 1975; Floyd and Leveridge 1987; Roser and Korsch 1988; Floyd et al. 1989; McLennan and Taylor 1991; Tortosa et al. 1991; Condie 1993; McLennan 1993; Hayashi et al. 1997; Cullers and Podkovyrov 2002; Gu et al. 2002; Mongelli et al. 2006; Bracciali et al. 2007; Nagarajan et al. 2007; Jinliang and Xin 2008; Schoenborn and Fedo 2011; Tao et al. 2017; Mahanta et al. 2020; Baral et al. 2021; Mudoi et al. 2022; Tiwari et al. 2023), tectonic setting (Dickinson and Suczek 1979; Dickinson et al. 1983; Dickinson 1985; Bhatia and Crook 1986; Roser and Korsch 1986; Toulkeridis et al. 1999; Gu et al. 2002; Jinliang and Xin 2008; Verma and Armstrong-Altrin 2013, 2016), source sediment weathering profile, and paleoconditions including paleoclimate and paleoredox environment (Suttner et al. 1981; Nesbitt and Young 1982, 1989; Suttner and Dutta 1986; Grantham and Velbel 1988; Jones and Manning 1994; Weltje 1994; Potter et al. 2005; Zhao et al. 2007; Galarraga

Supplementary Information The online version contains supplementary material available at https://doi.org/10.1007/s11631-025-00771-0.

✉ Yadav Krishna Gogoi
yadavkrishnagogoi@gmail.com

[1] Department of Petroleum Technology, Dibrugarh University, Dibrugarh, Assam, India

[2] Department of Applied Geology, Dibrugarh University, Dibrugarh, Assam, India

[3] Department of Geology, Pachhunga University College, Aizawl, Mizoram, India

et al. 2008; Ross and Bustin 2009; Cao et al. 2012; Ejeh 2021; Long et al. 2012; Roy and Roser 2013; Moradi et al. 2016).

The Gondwana sediments are exposed in both peninsular (i.e., Eastern and Central India) and extra-peninsular India (Sikkim and northeastern Arunachal Himalaya; Biswas 1999). Although the peninsular Gondwana sequences have received international and national attention (Acharyya 2019; Venkatachala and Tiwari 1987; Valdiya 1997; Wopfner and Jin 2009; Mukhopadhyay et al. 2010; Wang et al. 2021), the extra-peninsular part has not received much attention. Studies of sandstone geochemistry and petrography regarding the source, setting, and paleoclimatic conditions of the extra-peninsular Gondwana sequences have been published by various researchers (Priya et al. 2019; Mahanta et al. 2020; Gogoi et al. 2021). According to these petrographic and geochemical studies, the sediments originated in the interior of the cratons, and the bulk came from recycled orogeny with felsic igneous rocks as their source. Active continental margins, continental island arcs, and passive margin fields also acted as source areas of the detritus. The sediments underwent moderate to intense chemical weathering in humid paleoclimatic conditions during deposition. However, the implications from the above studies require deliberation, as the present study revealed some contrasting results, although some coherence with the previous works was found as well. The majority of the geological sections that have been studied are located in the West Kameng district of the Arunachal Himalayas (Gogoi et al. 2021). The Garu–Gensi Road sections parallel to the strike in the West Siang districts of the Arunachal Himalayas (Mahanta et al. 2020) and Sikkim-Darjeeling Himalayas (Priya et al. 2019) are among the other areas. The present research work was taken up to reconstruct the nature of sediment sources, their tectonic settings, and paleoclimate, paleoredox, and paleoweathering trends of newly exposed sandstones of the Gondwana Group rocks in parts of West Siang [along the Likabali–Garu–Basar (LB) Road section], East Siang [along the Pasighat–Rengging (PR) Road section], and lower Dibang valley [along the Bomak–Sisseri (BS) Road section] of the Arunachal Himalayas. In addition, paleoredox conditions were investigated because this had not been undertaken in any previous studies.

2 Geological setting of the study area

The Himalayan–Tibetan Orogeny was a result of the convergence of the Indian and Eurasian plates during the Cenozoic era (Hodges 2000; Najman et al. 2008; Ding et al. 2016). The NE–SW-trending Eastern Himalayas (Arunachal Himalayas) show a bend in the regional strike of the major litho-tectonic units towards NW–SE, terminating at the Namche Barwa syntaxis across the Siang gorge (Ding et al. 2001; Wadia 1931) (Fig. 1). This syntaxis is a NE-plunging antiform representing the Eastern Himalayan syntaxis which is composed of Higher Himalayan crystalline rocks (Choudhuri et al. 2009). The Indus-Tsangpo Suture Zone and the Trans-Himalayan plutonic band encircle the Namche-Barwa peak region in southern Tibet, exposing the crest of this syntaxis farther north (Burg et al. 1997) (Fig. 1). The South Tibetan Detachment System (STDS), a set of normal-sense faults and shear zones that run parallel to the orogeny, exposes the Tethyan sediments in places between the Trans-Himalayan rocks and Higher Himalayan crystalline (Yin 2006) (Fig. 1). The Higher Himalayan crystalline overrides the Lesser Himalayan crystalline along the Main Central Thrust (MCT) following the syntaxial bend (Choudhuri et al. 2009) (Fig. 1). In the eastern Arunachal Himalayas, the Siang antiform (Singh 1993) is located in the SW region of the Namche-Barwa Syntaxis (Fig. 1). This Siang antiform, plunging to the NNW, is a significant crustal-scale feature. It represents the subsurface indenture of the buckled Indian basement beneath the Asian Plate (Acharyya and Saha 2008). The Permian Gondwana Group rocks along with the younger Eocene rocks occupy the core of this Siang antiform. The Lesser Himalayan Sequence (LHS) marks the periphery of this antiform along the Bomdila Thrust (Sarma et al. 2020; Choudhuri et al. 2009) (Fig. 1).

The extra-peninsular Gondwana basin occupies the lesser Himalayan sequence of the Arunachal Himalayas in parts of the Garo-Basar area extending up to the Siang valley and in parts of the Sisseri River of Arunachal Pradesh as its northeastern-most limit (Fig. 1). This NE–SW-trending Gondwana sequence outcrops as discontinuous patches in linear belts along the Arunachal Himalayas (Kesari 2010). Its northern limit is bounded by Lesser Himalayan crystalline (Proterozoic) rocks, and the southern limit is defined by the Siwaliks Group (Miocene) rocks along the Main Boundary Thrust (MBT) in the Likabali–Basar Road section (Figs. 1 and 2). This road section exposes the Miri Formation and Bichom Formation of the Gondwana Group of rocks. The oldest Miri Formation comprises arenitic sandstones, quartzites, purple shale, and gray shale. The Miri Formation overrides the younger Bichom Formation along the Miri thrust near Daring village. The Bichom Formation comprises sandstone, carbonaceous shale with lenticular coal bands, gray shale, coal balls, and nodules within carbonaceous shale and gray shale bands, respectively. This formation has a thrust contact with the Miocene Dafla Formation along the MBT in this region (Fig. 2). A cross-fault trending NW–SE offsets the Miri and Bichom Formation along the Igo River in the region. In the Siang window, the Gondwana Group rocks are bounded by the younger Yinkiong Group (Paleocene–Eocene) rocks as faulted contact and Miocene Dafla Formation in the south along the Main Boundary Thrust (Fig. 3). The Bichom Formation of the

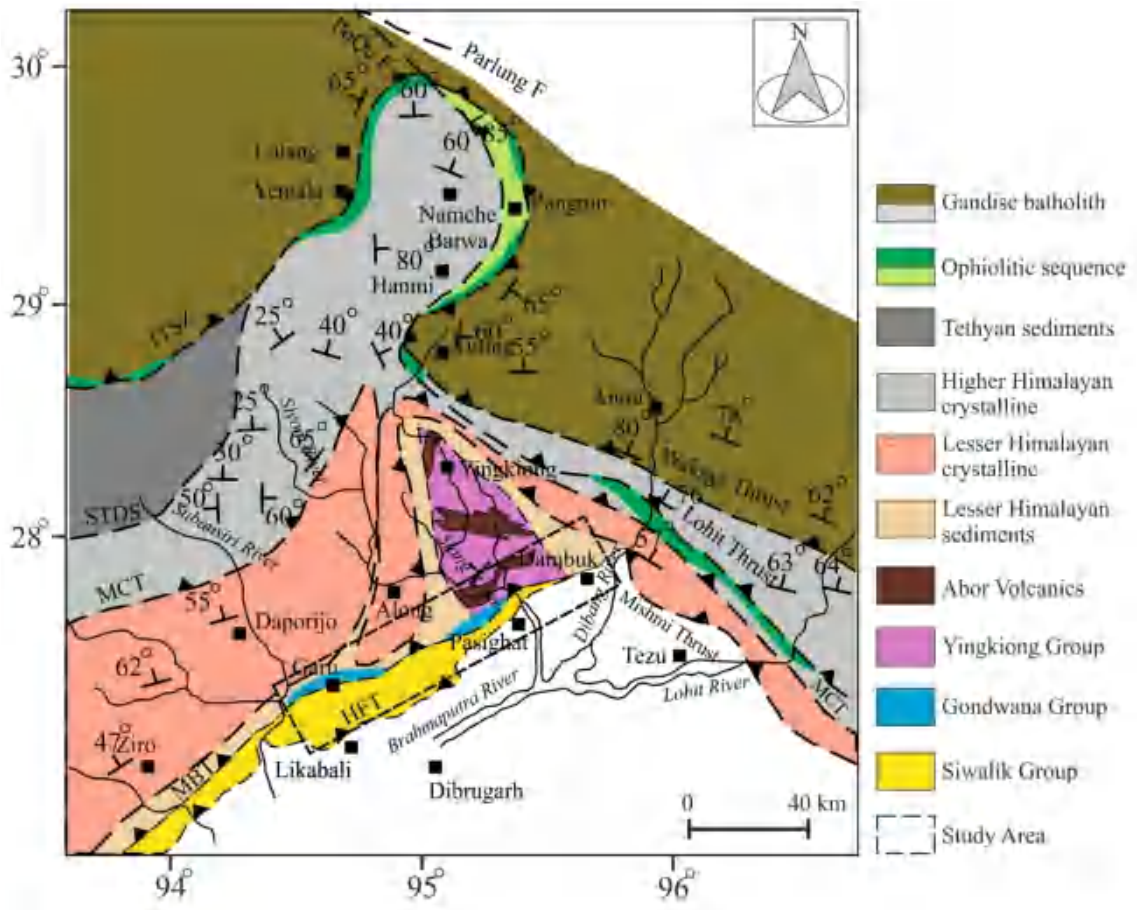

Fig. 1 Geological map showing the distribution of the Gondwana sequence in the eastern part of the Arunachal Himalayas (modified by Sharma et al. 2020; after Singh and Bikramaditya Singh 2012)

Lower Gondwana Group is exposed in this area along the right bank of Siang River. The oldest Miri Formation which strikes the frontal part of the Arunachal Himalayas in and around the Sisseri River over Quaternary deposits (terrace) marks the northeastern-most limit of the Gondwana Group rocks (Fig. 4). This formation mainly comprises arenitic sandstone, siltstone, quartzite, purple shale, gray shale, and limestone bands. These Gondwana sequences are occasionally cut by intrusive rocks which are both concordant and discordant in nature (Figs. 2, 3, 4, 5c, and d). A generalized stratigraphic succession (Table 1) of the Gondwana Group of the Himalayan belt is shown (Kesari 2010). The current study focuses on the sandstones of the Miri Formation and Bichom Formation of the Gondwana Group (Table 1).

3 Materials and methodology

A total of 19 and 24 representative sandstones were selected for petrographic and geochemical analysis, respectively. Rock thin sections were prepared from Araldite-impregnated sandstones and were used for the petrographic examination under a Leica DM750 P trinocular polarizing microscope with a CCD camera and Leica Application Suite (LAS) system. Using the Gazzi–Dickinson method, 500 points were counted per thin section to complete the modal count (Gazzi 1966; Dickinson 1970).

The geochemical analysis including major oxide, trace element, and rare earth element (REE) studies was carried out using X-ray fluorescence (XRF) and high-resolution inductively coupled plasma–mass spectrometry (HR-ICP-MS) at the National Geophysical Research Institute (NGRI), Hyderabad, India. Major oxide concentrations were measured using a Philips Magix PRO PW 2440 XRF instrument. Boric acid-filled sample pellets were prepared and distributed uniformly within the sample. After the pellets were subjected to pressing using a hydraulic compression machine, the main oxides in these pellets were measured. Five grams of each sample was heated to 800 °C to determine the loss on ignition (LoI), and both the initial and final weight were recorded. Using the approach described by Satyanarayanan et al. (2018), the sandstones

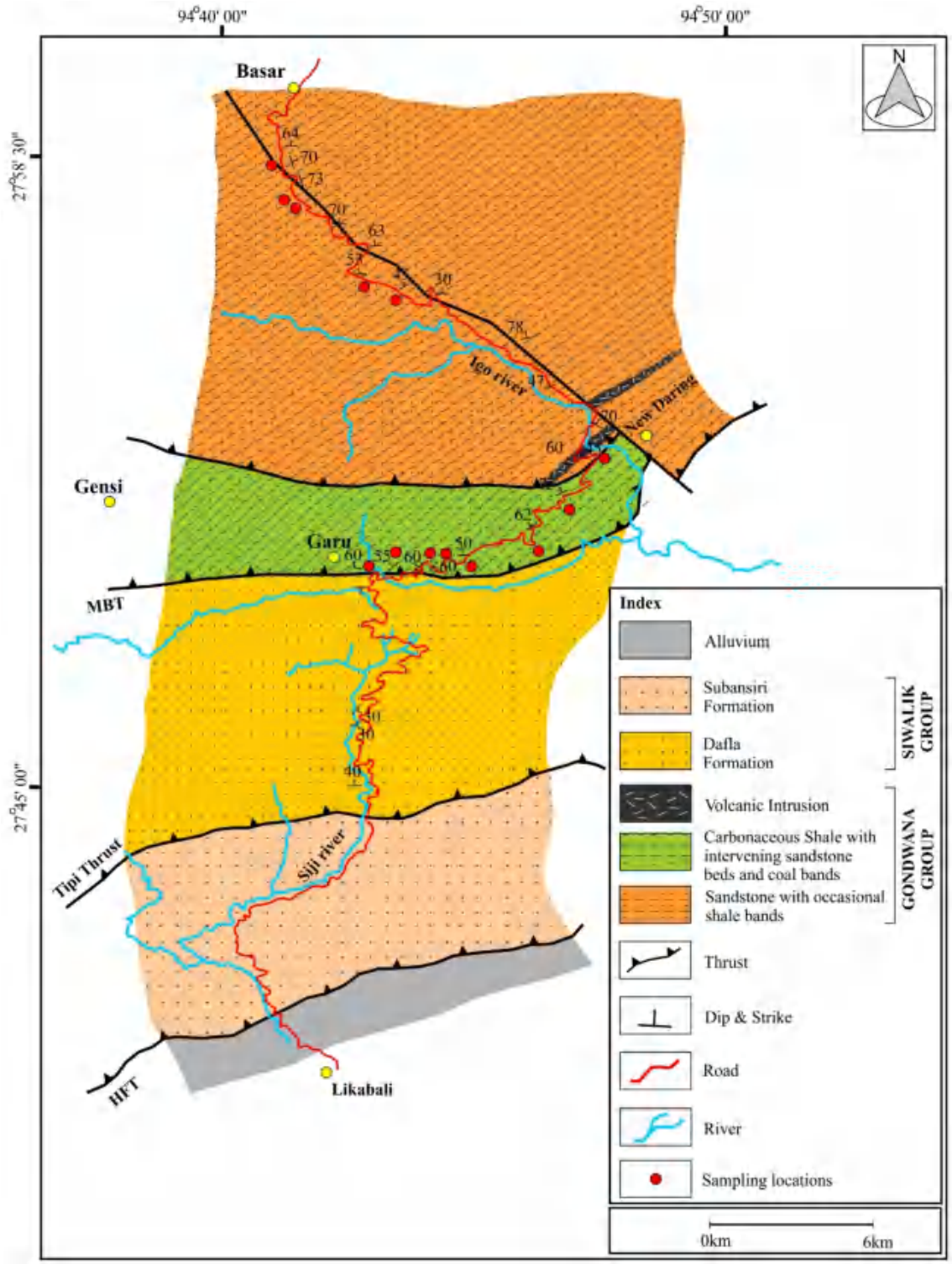

Fig. 2 Transect geological map along the Likabali–Garu–Basar (LB) Road section

underwent a wet chemical dissolution process for trace and rare earth element studies. Savillex screw-top vessels were filled with a test aliquot of each sample (0.05 g), followed by subsequent addition of an acid combination (10 mL of 7:3 HF-HNO_3) and internal standards (5 mL of 1 ng/mL ^{103}Rh). After a thorough swirling process, they were sealed tightly and incubated for 48 h at about 140 °C on a hot plate. To confirm that all of the HF had been eliminated

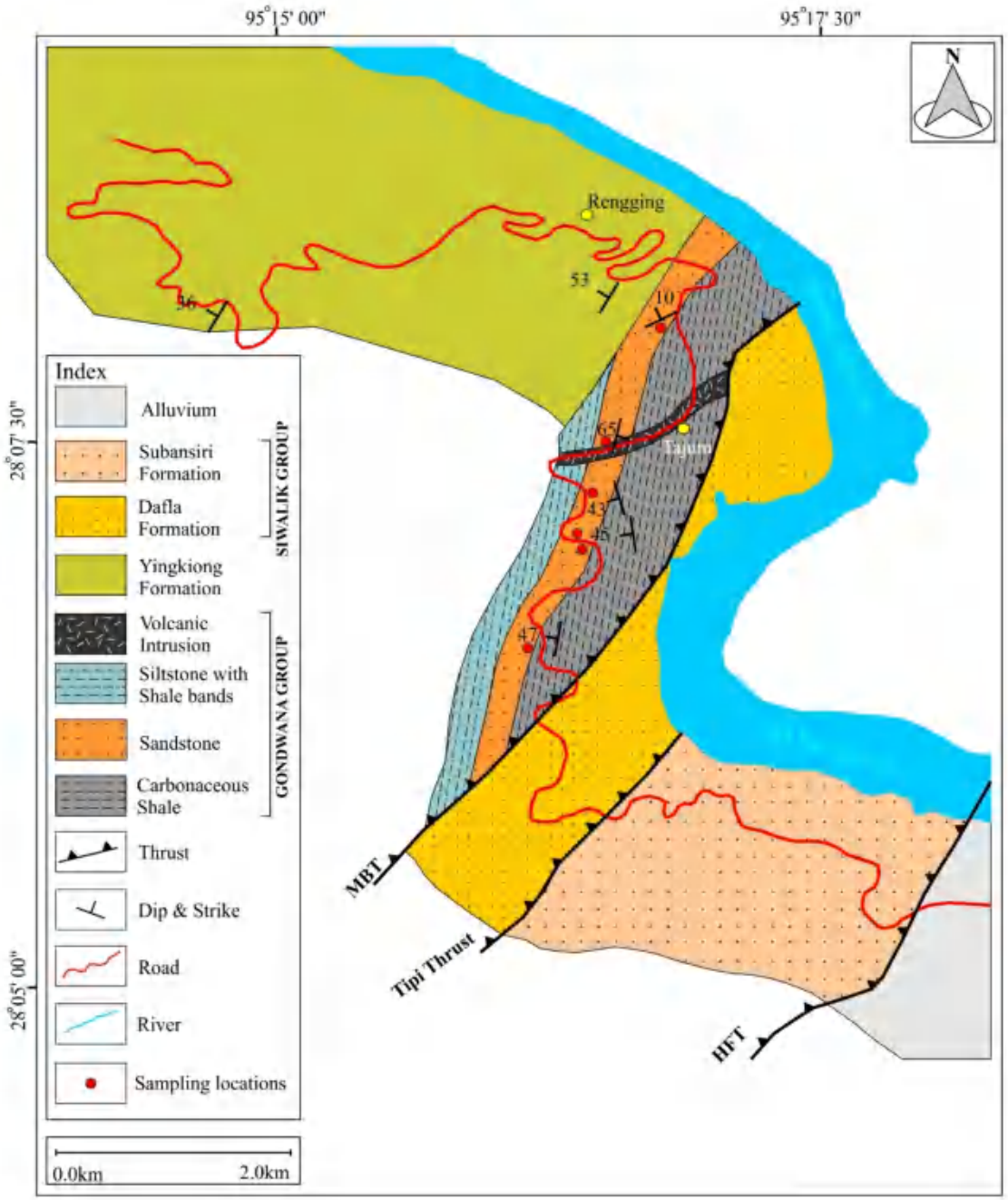

Fig. 3 Transect geological map along the Pasighat–Rengging (PR) Road section

from the mixture, the containers were then opened and the contents evaporated at 200 °C to almost dryness using a few drops of $HClO_4$. Finally, 10 mL of 1:1 HNO_3 was added to further dissolve the mixture and Milli-Q deionized water was added to bring the volume to 250 mL, after which the mixture was stored in high-density polyethylene (HDPE) bottles. Using the same procedure, a few procedural blanks were also prepared using the sample batch to eliminate handling and reagent errors. All trace elements had validated data for a subset of the geological reference samples. Every sample produced clear solutions, and the analysis was carried out using an Attom HR-ICP-MS with forward Nier–Johnson analyzer geometry (Nu Instruments, UK). Replica analyses of standards and samples were used to assess accuracy and precision, and the international reference sandstone sample (GSR-4) was used for calibration. The precision for the major, trace, and REE analyses was

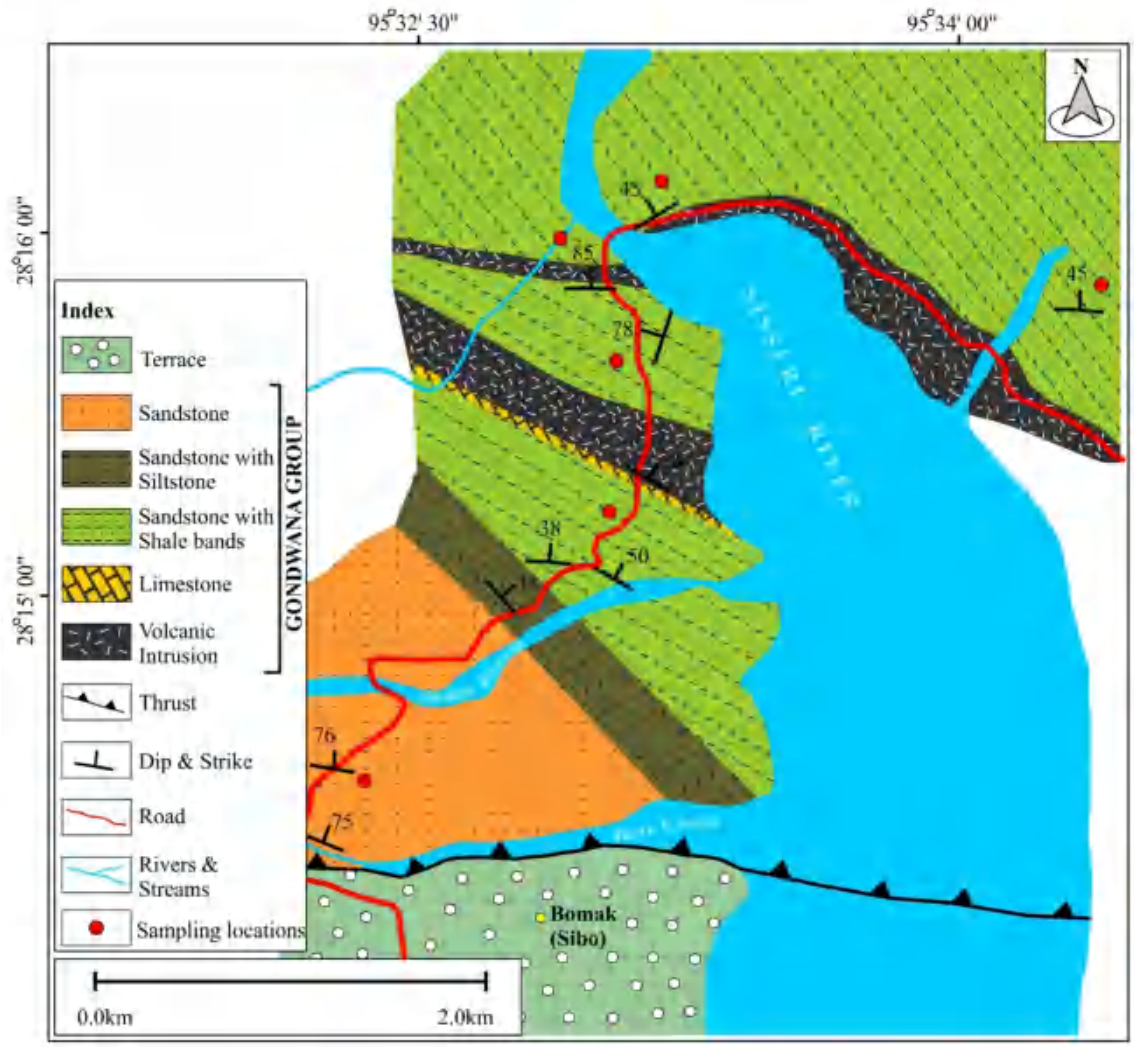

Fig. 4 Transect geological map along the Bomak–Sisseri (BS) Road section

determined to be < 2% RSD (relative standard deviation), with comparable accuracy.

4 Results

4.1 Petrography of sandstones

In the sandstones of the Gondwana Group, quartz is the dominant framework grain, represented by both mono- and polycrystalline varieties. Its concentration ranges from 15.34% to 97.20% (avg 65.16%). The monocrystalline variety comprises both non-undulatory types, with concentrations ranging from 0.00% to 31.11% (avg 13.53%), and undulatory types with concentrations varying between 2.79% and 77.73% (avg 44.88%), the latter variety being comparatively dominant. Volumetric percentages in the range of 0.00%–17.54% (avg 2.40%) for 2–3 units and 0.00%–21.04% (avg 4.36%) for more than three units per grain are recorded for the polycrystalline quartz. Sheared or stretched metamorphic quartz and recrystallized metamorphic quartz are typical among the polycrystalline variations. Plagioclase feldspar and K-feldspar (microcline) are two types of feldspar minerals that are observed, ranging from 0.00% to 9.20% (avg 1.38%) and 0.00% to 2.10% (avg 0.54%), respectively. The reported mica grains, mainly muscovite, are recorded in very small amounts (avg 0.11%). Rock fragments of igneous, sedimentary, and metamorphic varieties have been reported, ranging from 0.00% to 5.53%. Most of the grains are interlocked by cementing material (avg 1.33%) of silicious type, with ferruginous, argillaceous, and calcareous kinds also acting as binding agents. Matrix occupying pore spaces between grain boundaries is also present,

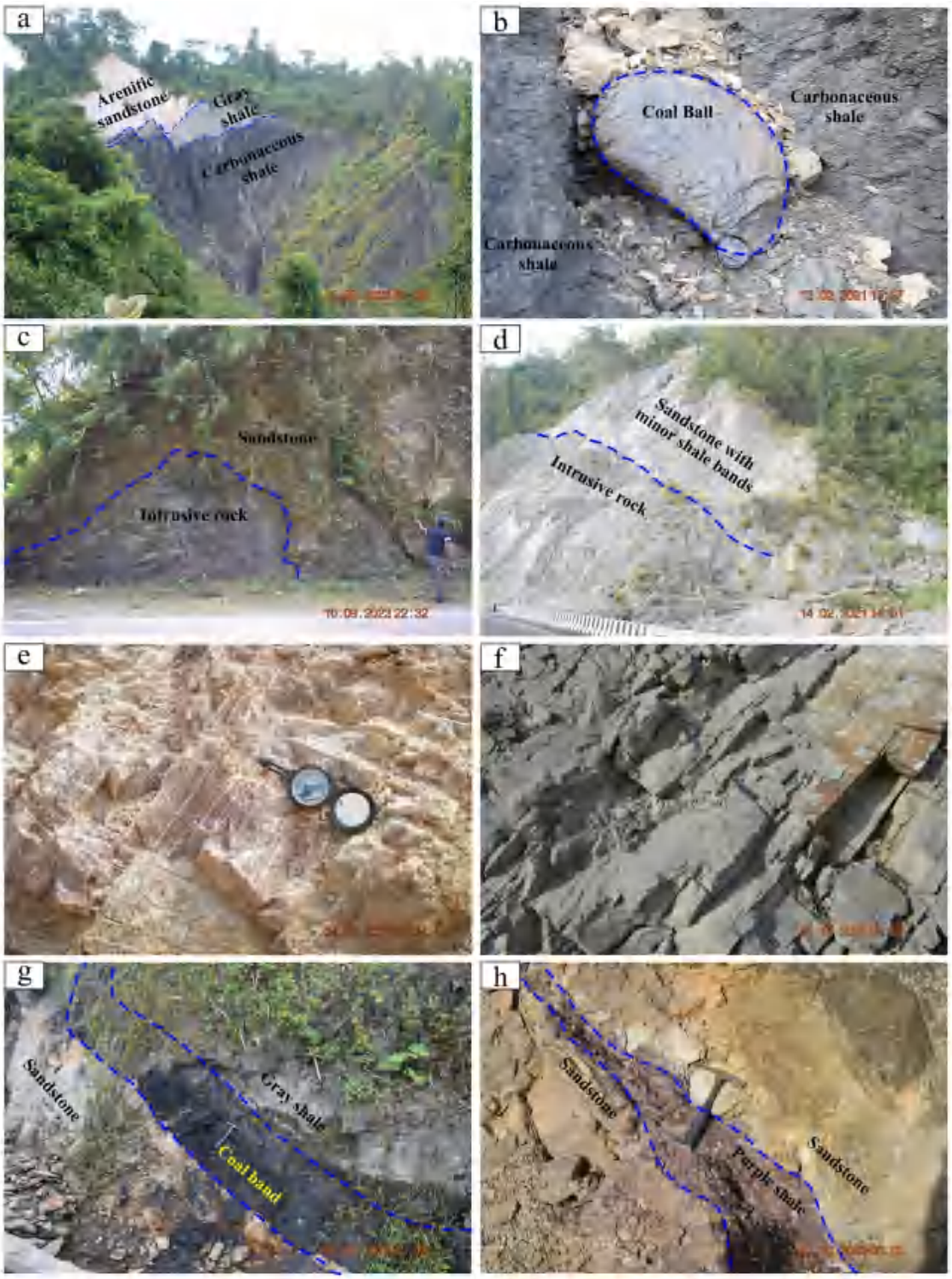

Fig. 5 Field photographs showing **a** association of carbonaceous shale, gray shale, and arenitic sandstone within the Gondwana sequence along the Pasighat–Rengging (PR) Road section; **b** coal ball within carbonaceous shale along the Pasighat–Rengging (PR) Road section; **c** discordant intrusive rock forcing into a siltstone bed along the Pasighat–Rengging (PR) Road section; **d** association of concordant intrusive rock with sandstone interbedded with minor shale bands along the Bomak–Sisseri (BS) Road section; **e** reddish-brown or brownish iron oxide banding in sandstone along the Likabali–Garu–Basar (LB) Road section; **f** grayish sandstone (medium-grained) along the Bomak-Sisseri (BS) Road section; **g** association of sandstone, coal bands, and gray shale within the Gondwana sequence along the Likabali–Garu–Basar (LB) Road section; **h** sandstone interbedded with purple shale along the Likabali–Garu–Basar (LB) Road section

Table 1 Stratigraphic succession of the Gondwana Group of the Himalayan Belt (Kesari 2010)

Group	Formation	Lithology	Age
Yingkiong Group			
Gondwana Group	Yamne Formation	Pale brown ferruginous shale	Upper Permian
	Abor volcanics	Porphyritic and aphyric basalt, andesite, Abor volcanic acidic tuffs, agglomerates, aquagene tuff, volcanic sediments	Permo-Carboniferous
	Bhareli Formation/ Khelong Formation	Upper member: feldspathic sandstone, black and carbonaceous shale with thin impersistent lenticular coal Lower member: arkosic red sandstone siltstone and black carbonaceous shale with thin impersistent lenticular coal	
	Lichi volcanics	Light to dark green basic volcanics	
	Bichom Formation	Sesa member: gray to black tuffaceous (?) shale with impersistent bands of quartzite Bomte member: Gray to black shale with calcareous and phosphatic chert nodules Rilu member: diamictite with subordinate sandstone, shale and grits	
	Miri Formation	Purple to pinkish, white to grayish white feldspathic quartzite, purple micaceous shale, diamictite conglomerate	Lower Paleozoic
Biotite granite			

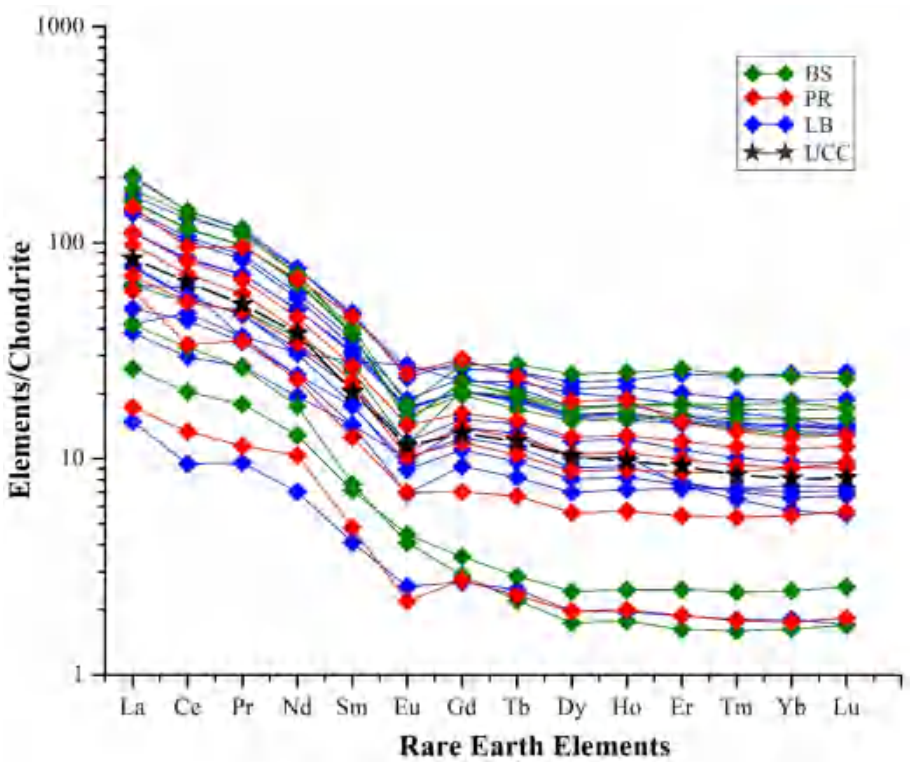

Fig. 6 Chondrite-normalized pattern of REE concentration

making up around 0.95% to 32.58% of the volume of the rock. One of the sandstones (LB 20) has detrital-source chert in it. Table 2 displays the corresponding percentages of all framework mineral grains. Additionally, detrital heavy minerals including zircon, tourmaline, sillimanite, kyanite, epidote, and andalusite are recorded along with the framework grains in the sandstones. The sandstones of the Gondwana Group are fine- to medium-grained, containing sub-angular to sub-rounded to well-rounded grains (Fig. 7). The sandstones are both quartz arenite and quartz wacke type. The arenites show moderately to well-sorted texture (Fig. 7b–d), whereas the wackes show poorly to moderately sorted texture (Fig. 7e, f, i). The arenites are texturally mature, which is supported by a quartz-dominated compact packing of framework grains,

Table 2 Volumetric weight percentage of framework grains of sandstones of the Gondwana Group

Sample	Quartz				Feldspar		Cement				Rock fragments			Matrix	Mica	Chert
	MNU	MU	P (2–3)	P > 3	Plagioclase	K-feldspar	Argillaceous	Ferruginous	Siliceous	Calcareous	Igneous	Sedimentary	Metamorphic			
PR 06	31.11	48.33	0.00	1.95	0.65	2.09	0.00	0.00	5.49	0.00	0.94	0.21	0.00	9.11	0.07	0.00
PR 07	22.60	46.95	0.00	1.73	0.86	0.00	0.00	0.00	0.00	0.00	0.00	2.48	0.00	22.98	2.36	0.00
PR 7A	26.17	55.62	0.00	1.83	1.43	0.65	2.48	0.00	10.60	0.00	0.00	0.65	0.00	0.52	0.00	0.00
PR 10	24.09	37.59	0.00	0.60	10.36	0.00	0.36	0.00	0.72	0.00	1.20	2.04	0.00	22.77	0.24	0.00
PR 14	55.11	38.77	0.00	1.83	0.00	0.916	0.00	0.00	0.45	0.00	0.00	1.52	0.00	1.37	0.00	0.00
BS 01	1.680	49.21	3.60	21.24	0.00	1.68	0.00	0.00	0.00	0.00	0.00	3.96	0.00	18.60	0.00	0.00
BS 07	10.83	76.10	3.91	0.00	1.69	0.00	0.78	0.00	0.00	0.00	0.00	0.78	1.04	4.83	0.00	0.00
BS 08	6.137	57.18	0.00	3.44	0.89	0.44	0.00	3.14	5.83	0.00	0.00	0.59	0.00	22.30	0.00	0.00
BS 11	11.84	62.93	4.89	3.34	2.57	0.00	0.00	0.00	1.67	0.00	0.00	5.53	0.00	7.20	0.00	0.00
LB 07	1.797	48.76	0.67	6.06	2.24	0.00	0.00	0.00	8.76	0.89	0.00	1.79	1.34	27.64	0.00	0.00
LB 11	20.59	26.23	18.23	17.69	0.22	0.00	1.60	0.22	7.85	0.00	0.00	2.05	0.00	5.26	0.00	0.00
LB 15	20.46	55.04	6.91	1.55	0.35	0.00	3.52	2.25	3.38	0.00	0.00	0.56	1.05	4.72	0.14	0.00
LB 16	32.39	4.70	0.00	2.07	0.94	1.12	0.00	0.00	0.56	22.59	1.69	1.31	0.00	32.58	0.00	0.00
LB 19	0.00	48.98	0.00	5.55	0.00	6.06	0.00	6.06	0.00	0.00	0.00	6.56	0.00	26.76	0.00	0.00
LB 20	3.50	34.08	0.98	9.26	1.43	0.53	0.44	7.82	30.66	0.00	0.00	1.79	0.00	8.27	0.17	0.98
LB 22	0.00	69.89	1.21	0.00	0.69	0.51	0.00	0.51	0.69	0.00	0.00	1.21	0.69	24.56	0.00	0.00
LB 24A	3.71	77.73	1.14	8.46	3.13	0.66	0.00	0.28	2.47	0.00	0.00	1.23	0.00	0.95	0.19	0.00
LB 29	0.00	63.49	0.00	2.77	1.78	0.00	0.00	0.00	0.00	0.00	1.58	0.99	0.00	29.36	0.00	0.00
LB 31	11.42	73.76	5.19	3.11	0.77	0.51	0.00	1.03	1.55	0.00	0.00	0.77	0.00	1.81	0.00	0.00

**NU* monocrystalline non−undulatory; *MU* monocrystalline undulatory; *P* polycrystalline; *PR* Pasighat−Rengging Road section; *BS* Bomak−Sisseri Road section; *LB* Likabali−Garu−Basar Road section

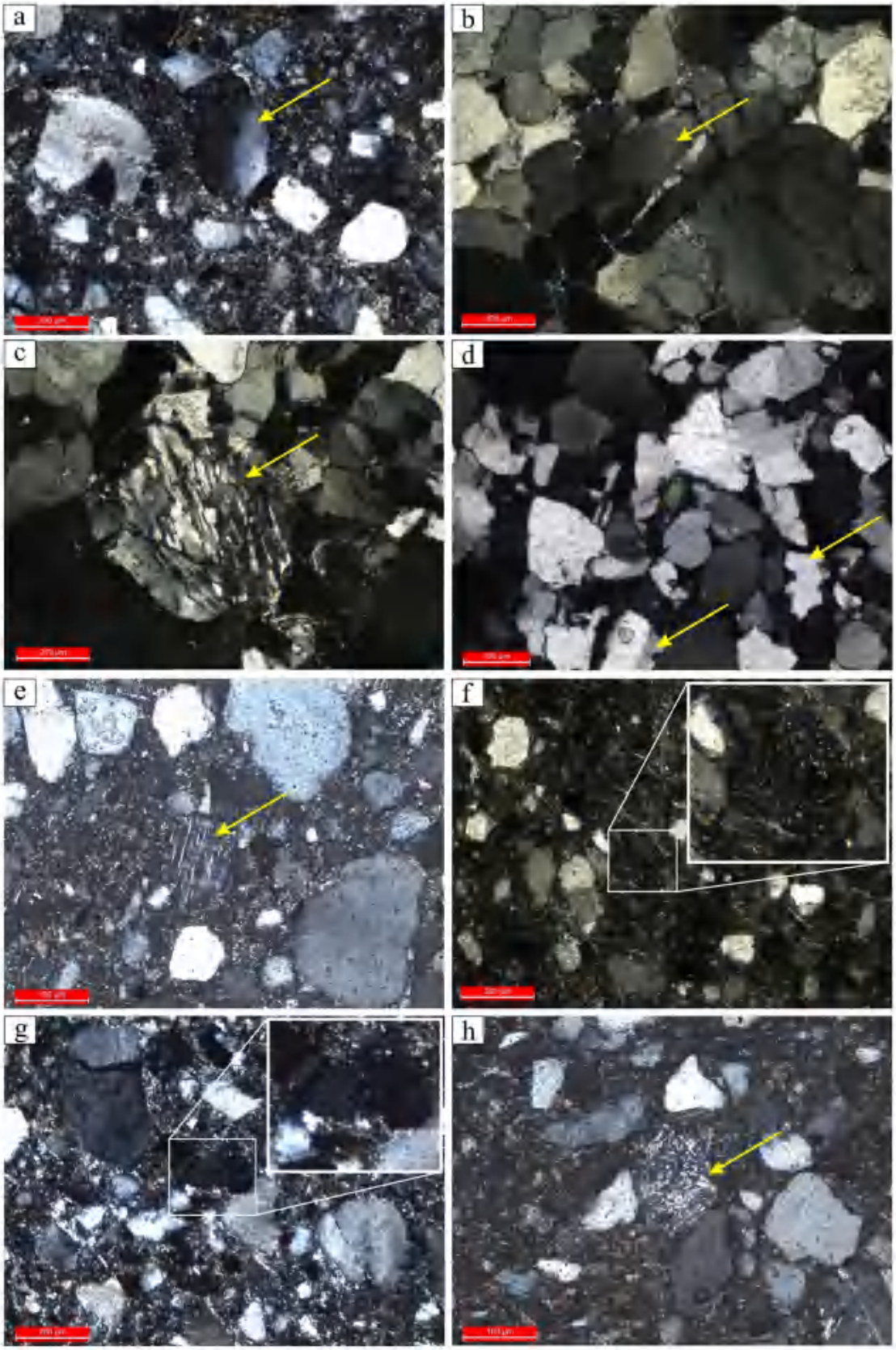
a
b
c
d
e
f
g
h

◀ **Fig. 7** Photomicrographs showing **a** undulatory monocrystalline quartz (yellow arrow); **b** composite or polycrystalline quartz (yellow arrow); **c** stretched metamorphic quartz (yellow arrow); **d** monocrystalline quartz with remnant embayments (yellow arrow); **e** K-feldspar or microcline; **f** myrmekite texture; **g** perthite texture; **h** igneous rock fragment (yellow arrow); **i** sedimentary rock fragment (yellow arrow); **j** metamorphic rock fragment (yellow arrow); **k** zircon (yellow arrow); **l** tourmaline (yellow arrow); **m** sillimanite (yellow arrow); **n** kyanite (yellow arrow); **o** epidote (yellow arrow); and **p** andalusite (yellow arrow)

whereas the immature wacke variety is supported by both quartz and matrix.

4.2 Chemical analysis of sandstones

4.2.1 Major oxides

The sandstones were investigated for major oxides, namely SiO_2, Al_2O_3, TiO_2, Fe_2O_3, MnO, Na_2O, K_2O, MgO, and CaO. Oxide composition in terms of weight percentage is shown in Table S4. These sandstones are marked by a higher concentration of SiO_2 (10.35–93.91wt%, avg 66.66 wt%), followed by the presence of Al_2O_3 (2.39–19.57 wt%, avg 9.10 wt%), CaO (0.05–31.17 wt%, avg 4.48 wt%), K_2O (0.05–9.47 wt%, avg wt 3.65%), Fe_2O_3 (1.06–6.64 wt%, avg 3.55 wt%), MgO (0.02–11.75 wt%, avg 2.82 wt%), TiO_2 (0.11–2.41 wt%, avg 0.69 wt%), Na_2O (0.05–1.77 wt%, avg 0.53 wt%), P_2O_5 (0.01–1.24 wt%, avg 0.21 wt%), and MnO (below detection limit, 0.43 wt%, avg 0.07 wt%). When comparing the average wt% of these sandstones with the wt% of UCC (Rudnick and Gao 2003), it is observed that they show enrichment in SiO_2, TiO_2, MgO, CaO, K_2O, and P_2O_5 concentration, while the remaining oxides, i.e., Al_2O_3, Fe_2O_3, MnO, and Na_2O, are depleted in nature.

Al_2O_3 shows a moderate positive correlation with K_2O ($R=0.57$) and TiO_2 ($R=0.38$) and a weak positive correlation with Na_2O ($R=0.27$), Fe_2O_3 ($R=0.23$), SiO_2 ($R=0.06$), and P_2O_5 ($R=0.05$), whereas it is negatively correlated with CaO ($R=-0.36$), MgO ($R=-0.30$), and MnO ($R=-0.04$). A positive correlation of these oxides indicates their enrichment due to their association with rock fragments and/or clay minerals, while a negative correlation indicates alteration and/or leaching during sedimentation processes (Nagarajan et al. 2007). Again, the correlation of Fe_2O_3 versus TiO_2 shows a moderate positive correlation ($R=0.50$), implying an enrichment of both elements due to the presence of Fe- and Ti-bearing heavy minerals and/or diagenetic enrichment of iron (Baioumy 2014).

4.2.2 Trace elements

The analytical results of the trace elements recorded in the sandstones have been summarized in Table S5, and a comparison of their enrichment/depletion with respect to the UCC (Rudnick and Gao 2003) is shown. Large-ion lithophile elements (LILE) recorded include Rb (avg 96.92 ppm), Sr (avg 88.772 ppm), and Ba (avg 304.97 ppm), among which Rb is enriched and both Sr and Ba are depleted in nature. The recorded high-field-strength elements (HFSE) Th (avg 15.53 ppm), Hf (avg 8.33 ppm), and Zr (avg 266.6 ppm) are enriched, while U (avg 1.97 ppm) is depleted. Transition elements including Sc (avg 8.45 ppm), V (avg 62.95 ppm), Cr (avg 33.878 ppm), Co (avg 5.91 ppm), Ni (avg 19.90 ppm), Cu (avg 16.02 ppm), Zn (avg 16.72 ppm), and Pb (avg 6.58 ppm) are depleted, whereas Y (avg 29.98 ppm) and Nb (avg 12.857 ppm) are enriched similarly to UCC (Rudnick and Gao 2003).

4.2.3 Rare earth elements (REE)

The concentration of lanthanides, i.e., REE (from La-Lu) is shown in Table S5 and is compared with the REE concentration of UCC. The REE can be divided into light rare earth elements (LREE: La-Gd) and heavy rare earth elements (HREE: Tb-Lu). The chondrite-normalized pattern of REE concentration (Fig. 6) shows a pattern similar to the UCC (normalized with chondrite concentrations), where LREE is enriched over HREE. The enrichment is indicated by strong fractionation of LREE over weak fractionation of HREE represented by a flat pattern. The LREE/HREE ratio ranges from 5.17 to 16.31 (avg 12.788). The chondrite-normalized ratio $(La/Yb)_N$ ranges from 2.72 to 25.64 (avg 9.43), $(Gd/Yb)_N$ ranges from 1.05 to 2.41 (avg 1.51), and $(La/Sm)_N$ ranges from 1.49 to 4.77 (avg 3.80). These values are similar to the UCC values (Taylor and McLennan 1985). The negative Eu anomaly (Eu/Eu*: avg 0.67), which shows an analogous pattern to UCC, is indicative of fractionation of feldspar at the source. A Ce anomaly is a prominent indicator of paleoredox deposition conditions, as it is redox-sensitive. The studied sandstones have a Ce anomaly ranging from 0.71 to 1.25 (avg to 0.92).

5 Discussion

5.1 Provenance

The optical characteristics of framework grains such as quartz, feldspar, and lithic fragments are reliable source indicators. The optical properties and polycrystallinity of quartz, along with the feldspar types, provide valuable insights into their igneous and metamorphic sources. Moreover, lithic fragments also act as direct indicators of their source. The dominance of undulatory and non-undulatory monocrystalline quartz over polycrystalline quartz in the examined sandstones indicates plutonic and low-rank metamorphic origins (Folk 1980). Strained quartz with strong undulatory

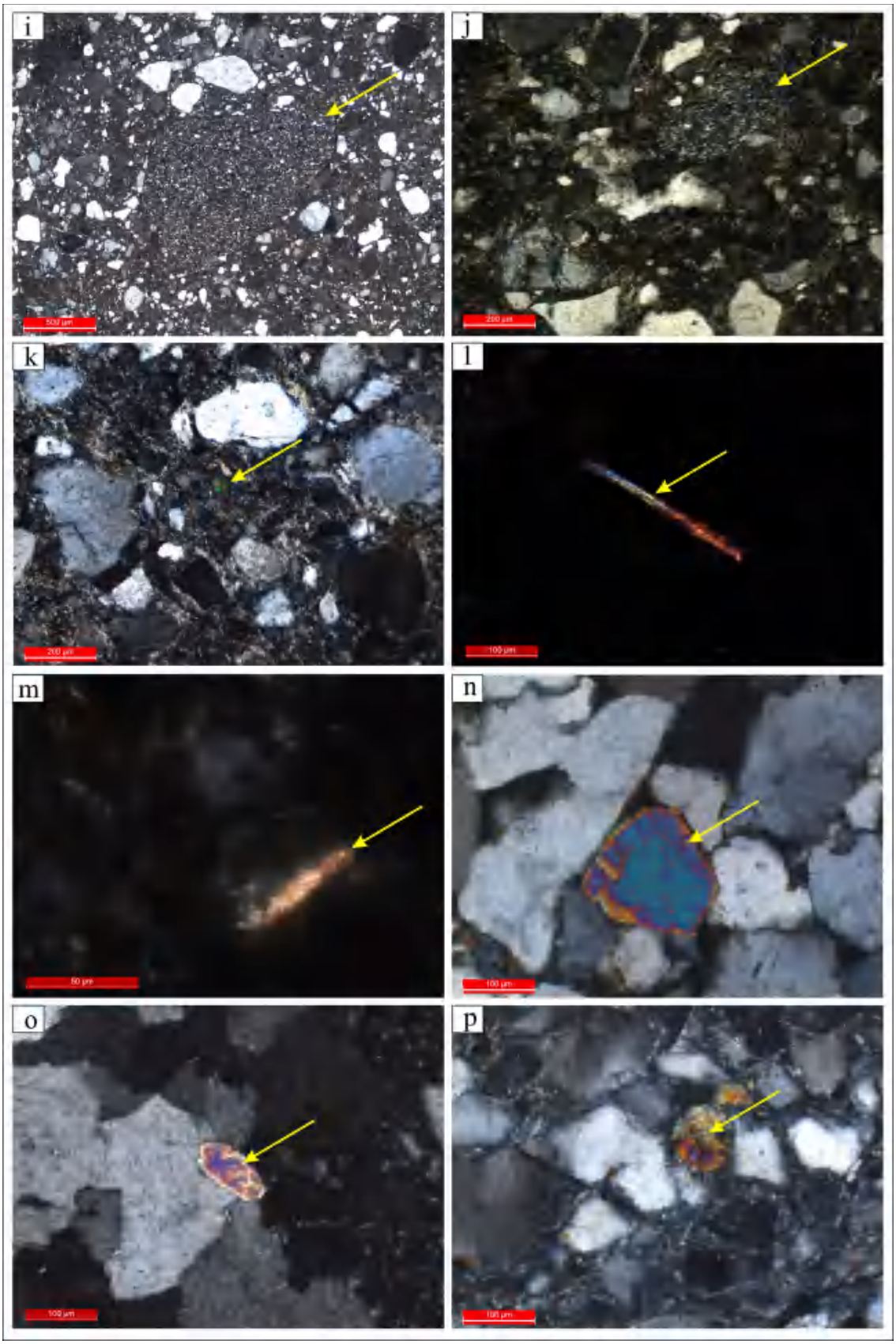

Fig. 7 (continued)

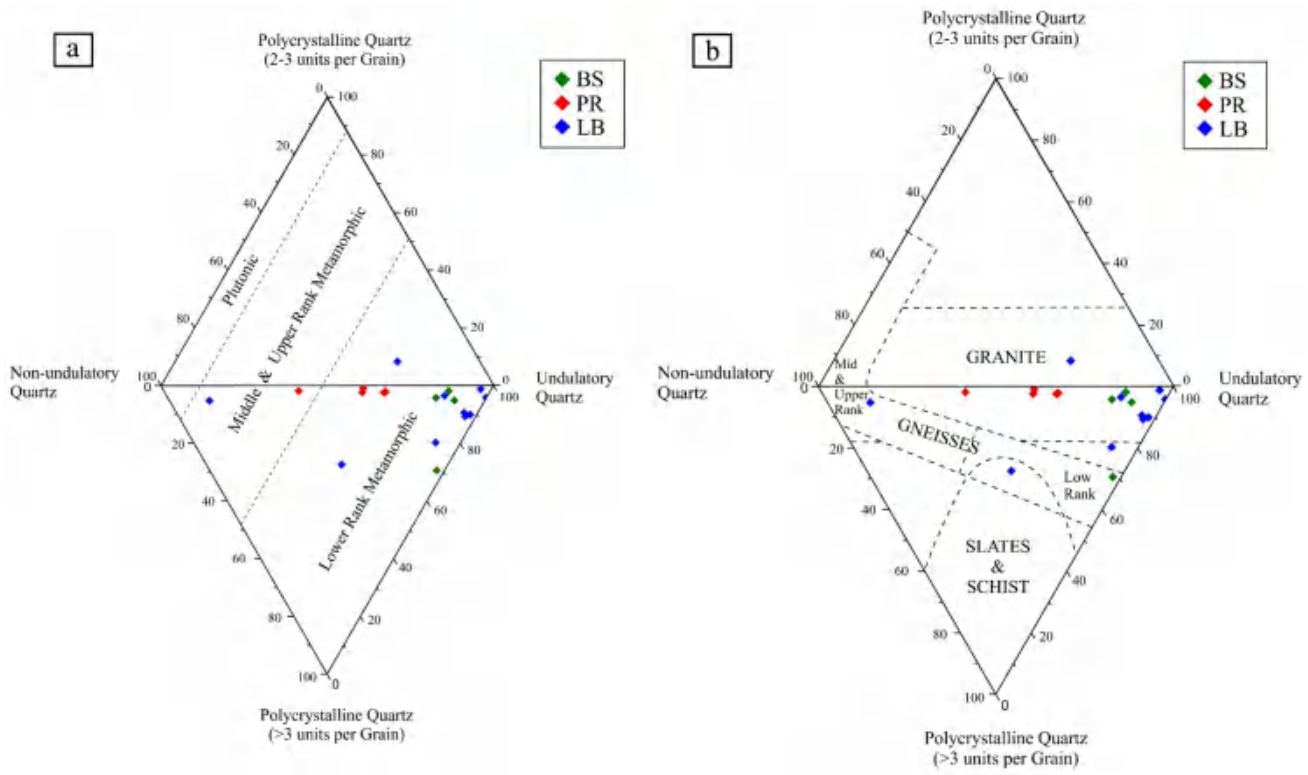

Fig. 8 **a** Diamond discrimination plot after Basu et al. (1975) indicating low/mid/upper-rank metamorphic rocks as source of sediments for the sandstones of the Gondwana Group. **b** Diamond discrimination plot after Tortosa et al. (1991) indicating granitic and low-rank metamorphic rocks as source of sediments for the sandstones of the Gondwana Group

extinction is observed where rocks are subjected to compression during in situ burial (Basu 1985). However, terranes with considerable deformation or metamorphism also act as sources of quartz that have suffered dislocations in the crystal lattice (Basu 1985). The undulatory quartz (Fig. 7a) observed here may be indicative of a metamorphic source. Composite or polycrystalline quartz (Fig. 7b) is indicative of both igneous and metamorphic origin. However, polycrystalline quartz (Fig. 7c) exhibiting elongation of their crystal lattices with sutured internal boundaries can be referred to as detrital stretched quartz of metamorphic origin (Krynine 1946; Folk 1980). In the present study, monocrystalline quartz with remnant embayments with rounded corners have been observed (Fig. 7d), which indicate detrital quartz of volcanic source (Krynine 1946; Folk 1980). Detrital feldspar also functions well as a source indicator. The K-feldspar or microcline (Fig. 7e) found in this study suggests their origin from igneous and metamorphic rock (Halder 2020). Additionally, intergrowth textures such as myrmekite (Fig. 7f) and perthite (Fig. 7g) point to the source of igneous rock. Rock fragments originating from lithotypes may inherit their compositional and textural attributes of the parent rock if not dissolved. Lithic fragments of igneous, sedimentary, and metamorphic origin observed in the present study confirm their respective sources (Fig. 7h–j). Heavy minerals are good indicators of provenance (Sengupta 1994; Morton 1985). The recorded heavy minerals in the rock thin sections of the sandstones indicate a mixed nature of sources including acidic to intermediate igneous rocks and low- to high-grade metamorphic rocks. The presence of zircon grain (Fig. 7k) suggests derivation from silicic and intermediate igneous rocks (Mange and Maurer 1992). The tourmaline (Fig. 7l) recorded may be sourced from acid igneous rock or granite pegmatites (Sengupta 1994; Mange and Maurer 1992). The presence of sillimanite (Fig. 7m), kyanite (Fig. 7n), epidote (Fig. 7o), and andalusite (Fig. 7p) points to low/high-grade metamorphic rocks like schists and gneisses (Mange and Maurer 1992).

In addition, quantified framework grains when put into discrimination diagrams provide insights into the nature of their source rock. Basu et al. (1975) and Tortosa et al. (1991) extensively addressed the use of quartz grains and their polycrystalline varieties to determine their sources. The ternary discrimination diagram developed by Basu et al. (1975) suggests that the sources are mostly from lower-rank metamorphic rocks, with some originating from medium- and upper-rank metamorphic rocks (Fig. 8a). Furthermore, Tortosa et al. (1991) modified the aforementioned

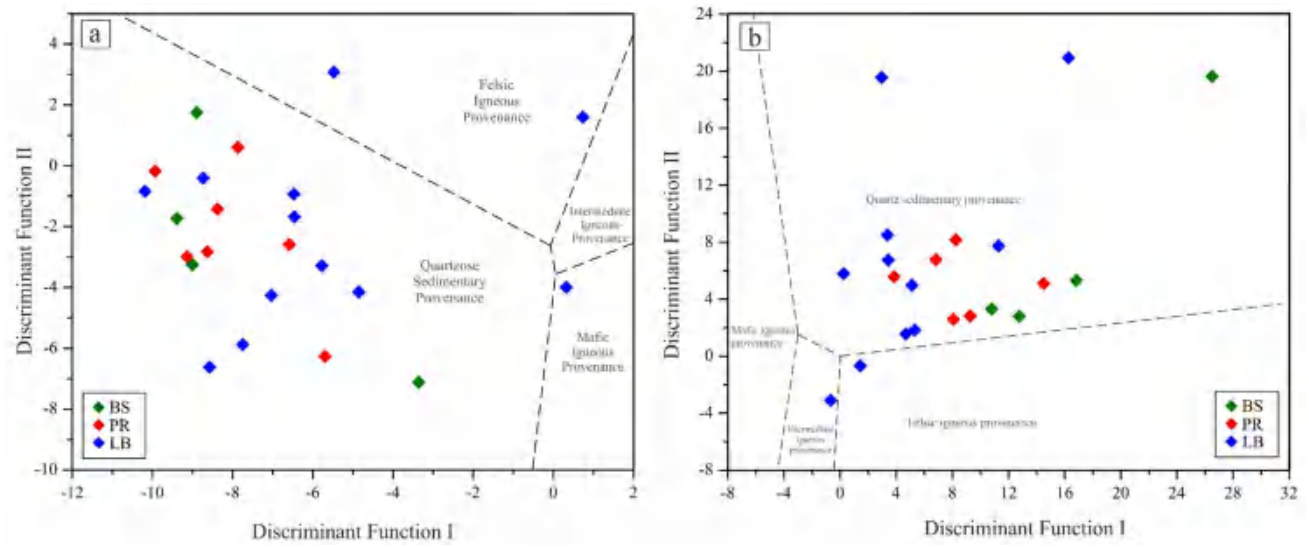

Fig. 9 **a** Provenance discriminant plot (discriminant function I versus discriminant function II) for sandstones of the Gondwana Group based on major oxide concentration (Roser and Krosch 1988). **b** Provenance discriminant plot (discriminant function I versus discriminant function II) for sandstones of the Gondwana Group based on major oxide ratios (Roser and Krosch 1988)

discrimination diagram. Using this discrimination diagram, the sandstones show that the sources are granites, with minor inputs from metamorphic rock of lower, middle, and upper rank (Fig. 8b). This corroborates the results from Gogoi et al. (2021).

Major oxide analysis is an important tool for discriminating various sediment sources by determining their concentrations (in wt%) and ratios using discriminant functions. Roser and Krosch (1988) proposed these discriminant functions (discriminant function I and discriminant function II) to separate felsic igneous rocks, intermediate igneous rocks, mafic igneous rocks, and quartzose sedimentary rocks from each other. About 90% of the sandstones (Fig. 9a and b) in the present study correspond to their derivation from the quartzose sedimentary provenance category, with the remaining belonging to the felsic, intermediate, and mafic igneous rock groups. Contrasting inferences were reported by Mahanta et al. (2020), where a felsic igneous provenance was found to be the majority source of the sediments. The indication of a vast majority of quartzose sedimentary origins of the sandstones in this study can be attributed to sediments that originated in mature continental regions. This may be facilitated by sources such as highly worn granites or gneisses, or it may have been derived from a previous sedimentary provenance (Roser and Krosch 1986). Moreover, enrichment of Zr (Table S5) in trace element study supports the fact that sediment recycling is a direct indication of quartzose sedimentary provenance (Zimmermann and Bahlburg 2003).

Elements such as Ca, K, Mg, and Na often leach out to a certain degree during source rock weathering. But elements like Al, Ti, and Zr intrinsically inherit their parent rock composition without undergoing any kind of leaching. This is because their oxides and hydroxides have very low solubility in low-temperature aqueous solutions (Palmer and Wesolowski 1992). Thus, the ratio of Al_2O_3/TiO_2 is quantitatively nearly equivalent to the rocks that served as their source (Garcia et al. 1994; Girty et al. 1996; Hayashi et al. 1997). The range of ratio values of felsic, intermediate, and basic igneous rocks are > 21, 8–21 and < 8, respectively (Roser and Krosch 1988). Garcia et al. (1994) and Hayashi et al. (1997) delineated the ranges as 21–70, 8–21, and 3–8 for felsic, intermediate, and basic igneous rocks, respectively. The Al_2O_3/TiO_2 values of the studied sandstones range from 3.51 to 44.76 (avg 19.20). The bulk of the examined sandstone sediments were produced from felsic and intermediate igneous rocks, with some contributions from basic/mafic igneous provenance as well, as presented in the bivariate plot of Al_2O_3 versus TiO_2 (Krzeszowska 2019; Fig. 10). The Zr versus TiO_2 bivariate discrimination plot and TiO_2/Zr ratio can also be used as a proxy to characterize the composition and nature of source rock (Hayashi et al. 1997). With the enrichment of SiO_2 concentration, the TiO_2/Zr wt% ratio often falls below > ~200, 195–55, and < 55 for mafic, intermediate, and felsic igneous rocks, respectively (Hayashi et al. 1997). The bivariate plot of Zr versus TiO_2 (Fig. 11a) of the present studied sandstones after Hayashi et al. (1997) indicates that most sediments are sourced from felsic igneous rocks, with fair inputs from intermediate igneous rocks. This inference is well supported by the TiO_2/Zr wt% ratio (Table S7). The Al_2O_3 versus TiO_2 bivariate plots indicate the sources to be felsic and intermediate rocks, with some mafic inputs. This

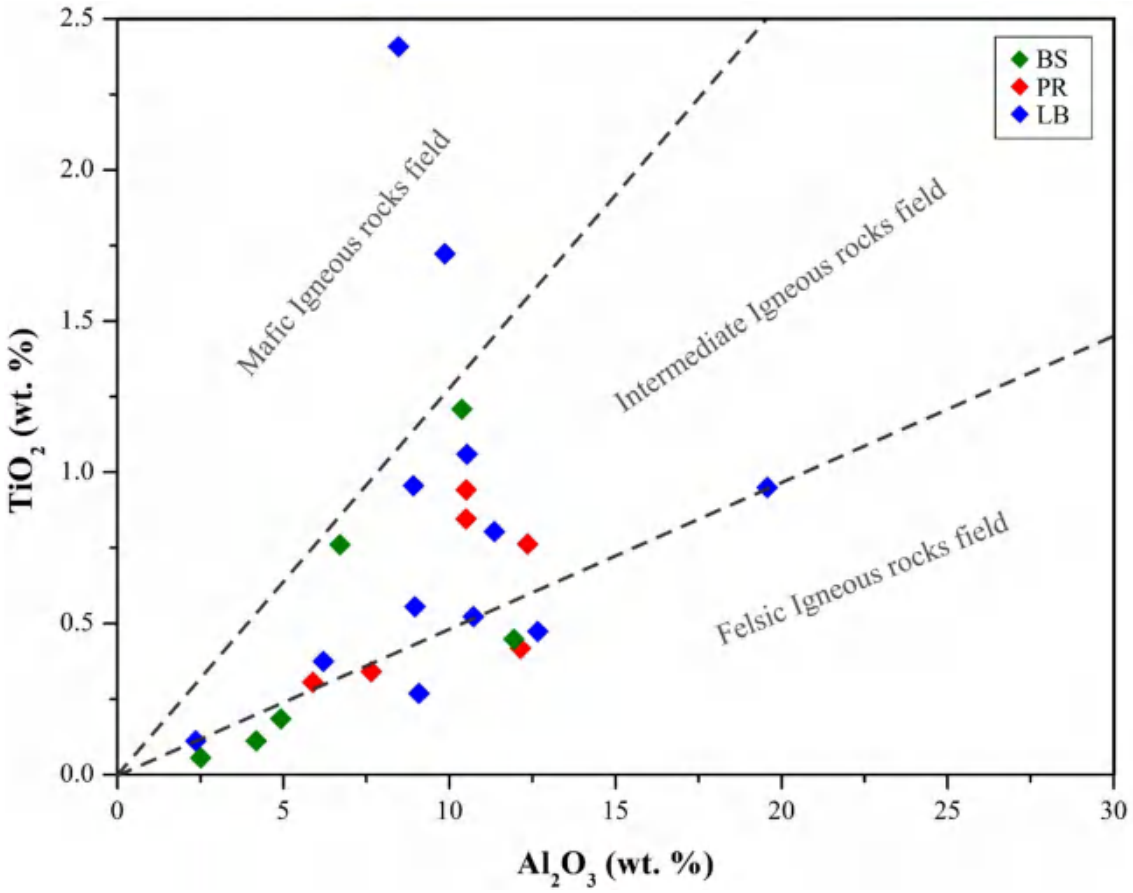

Fig. 10 Bivariate discrimination plot of Al_2O_3 versus TiO_2 (Krzeszowska 2019) depicting the nature of source rocks for sandstones of the Gondwana Group

is not entirely consistent with the Zr versus TiO_2 plot and TiO_2/Zr ratio. Thus, there is a certain degree of discrepancy. This variation can be attributed to the fractionation of TiO_2- and Zr-containing minerals commonly associated during transit and deposition of clastic rocks (Hayashi et al. 1997). Furthermore, relatively immobile elements like Ti and Ni can be used to differentiate juvenile sediments originating from magmatic precursors from normal mature sediments, providing an additional chemical check on the initial lithological composition (Floyd et al. 1989). Figure 11b shows that the studied sandstones are clustered against an acidic and magmatogenic graywacke field and are indicative of acidic and intermediate igneous rocks as sources.

Trace element and REE chemical characteristics are important tools for determining the distinctive nature and source composition of sediments. Their immobility and finite fractionation aids in precise determination using their concentrations in various bivariate and ternary discrimination plots (Shaw 1968; Floyd and Leveridge 1987; Floyd et al. 1989; McLennan and Taylor 1991; McLennan 1993; Hayashi et al. 1997; Cullers and Podkovyrov 2002; Mongelli et al. 2006; Bracciali et al. 2007; Jinliang and Xin 2008; Tiwari et al. 2023). Trace elemental ratios including europium anomaly (Eu/Eu*), La/Sc, La/Co, Th/Sc, Th/Co, and Th/Cr are universally used to derive the source region's provenance composition (Cullers et al. 1987, 1988; Cullers and Stone 1991; Cullers 1994a, b, 2000; Cullers and Podkovyrov 2002; Armstrong-Altrin et al. 2004). The range of elemental ratios of the studied sandstones are compared with those of sediments derived from felsic and basic rocks in similar fractions (Cullers 2000). The comparison points to the dominance of felsic source rocks over those from mafic source rocks (Table S6). Phillips et al. (2017) proposed the Th/Sc ratio to represent different source rock fields, where values ≥ 1 are typical of continental crust enriched in incompatible elements, ≥ 0.6–1 indicates an andesitic composition, and < 0.6 indicates a mafic signature. The majority of the studied sandstones have a Th/Sc ratio ≥ 1, with two exceptions falling within ≥ 0.6–1 and < 0.6 (Table S5). Thus, they are indicative of sediments derived from continental crust enriched in incompatible elements with minor inputs from andesitic and mafic rocks. In addition, elevated

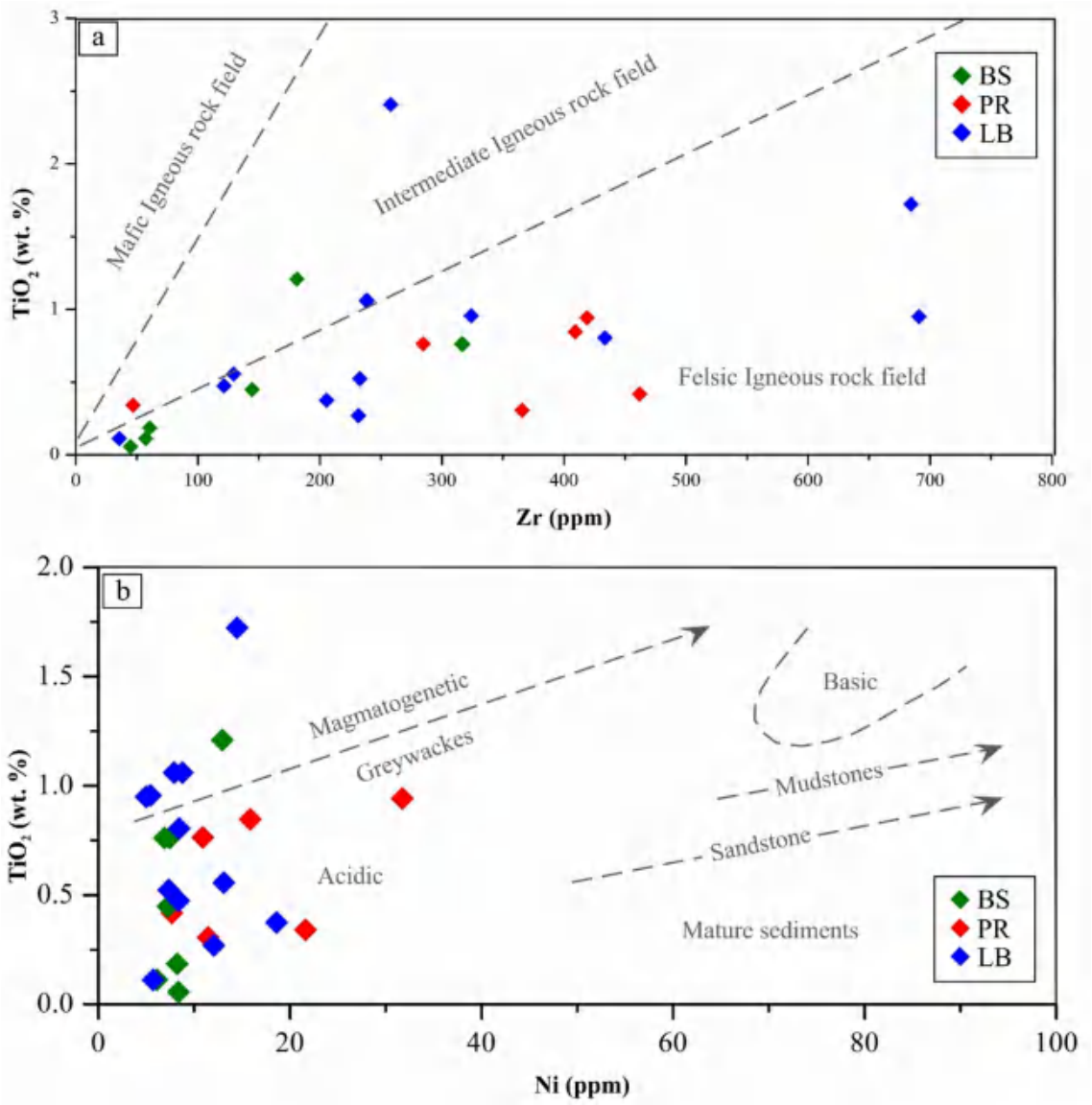

Fig. 11 **a** Bivariate plot of Zr versus TiO_2 (Hayashi et al. 1997); **b** bivariate plot of Ni versus TiO_2 (Floyd et al. 1989). Both plots depict the nature and composition of parent rocks for the sandstones of the Gondwana Group

concentrations of ferromagnesian trace elements such as Cr and Ni (where Cr > 150 ppm and Ni > 100 ppm) and a Cr/Ni ratio in the range of 1.3–1.5 indicate an ultramafic rock source (Garver et al. 1996). The lower threshold concentrations of Cr and Ni and lower Cr/Ni ratio of the studied sandstones indicate the absence of ultramafic rocks as source, with the exception of one sample with elevated Ni concentration (Table S5).

The REE pattern (chondrite-normalized) and Eu anomaly provide insights into possible source rock characteristics of sedimentary rocks (Basu et al. 1975; Taylor and McLennan 1985; Armstrong-Altrin 2009; Armstrong-Altrin et al. 2013). Cullers (1994a, b) proposed that a high LREE/HREE ratio and negative Eu anomaly (< 1) indicated felsic source rocks, while rocks of a mafic source exhibit a low LREE/HREE ratio and no Eu anomaly. The enrichment of fractionated LREE with unfractionated HREE, pronounced negative Eu anomaly (Eu/Eu* = 0.67; Fig. 6), and higher LREE/HREE (avg 12.78; Table S5) of the studied sandstones indicates that their source is likely of felsic nature. The Sm/Nd ratio acts as an alternative source indicator in the absence of Sm and Nd isotope analysis (Worash and Valera 2002). This is because the Sm/Nd ratio is close in proportionality to the $^{147}Sm/^{144}Nd$ ratio (Andre et al. 1986; Banner et al. 1988). Faure (1986) estimated the Sm/Nd ratio of rocks with granitic composition to be 0.19. The Sm/Nd ratio (avg 0.19; Table S5) of the studied sandstone complements the designated ratio and indicates granitic parent rock.

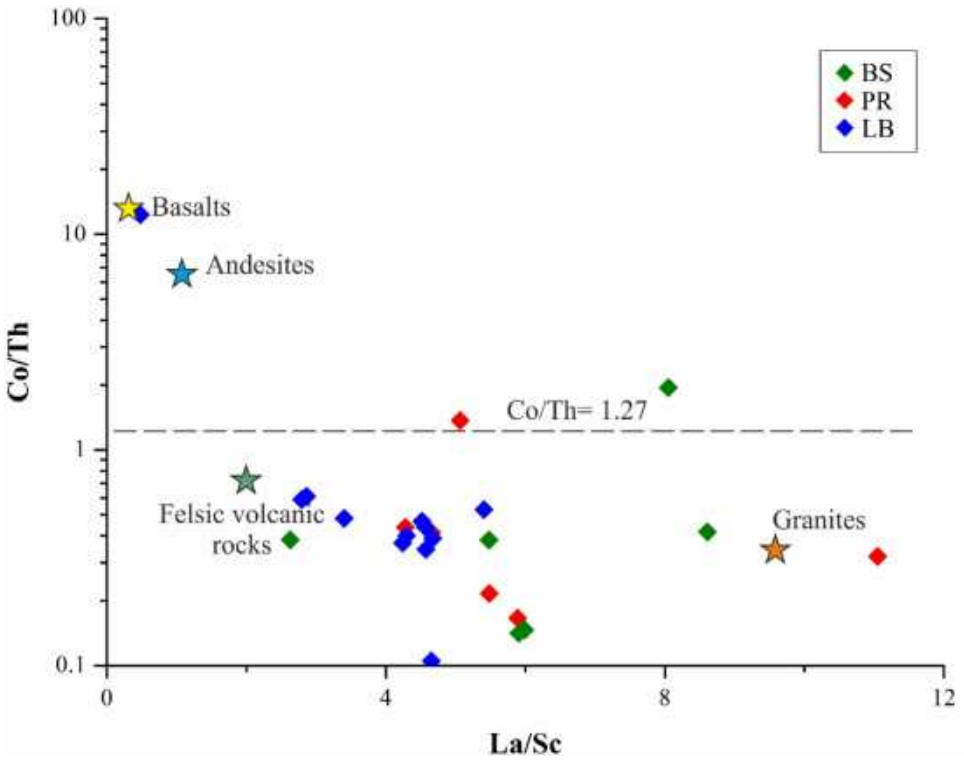

Fig. 12 Bivariate plot of La/Sc versus Co/Th (Gu et al. 2002) discriminating the source rock for the sandstones of the Gondwana Group

Apart from considering elemental concentration and their ratios, researchers (Gu et al. 2002; Mongelli et al. 2006; Bracciali et al. 2007; Jinliang and Xin 2008; Schoenborn and Fedo 2011; Tiwari et al. 2023) have widely used various discrimination diagrams in the form of bivariate and ternary plots considering both trace element and REE for source rock evaluation. A bivariate plot of La/Sc versus Co/Th (Gu et al. 2002) separates felsic volcanic rocks and granites from mafic (basalts) and intermediate (andesite) rocks with an elemental ratio of Co/Th = 1.27. The predominant clustering of the studied sandstones within the felsic volcanic rocks and granites supports their source with two sandstones in the region of intermediate source as well (Fig. 12). Intermixing of Y/Ni and Cr/V provides source characteristics where Y/Ni represents granitic rocks and Cr/V represents ultrabasic rocks (Mongelli et al. 2006). The bivariate plot of Y/Ni versus Cr/V of the sandstones indicates their source to be of granitic composition (Fig. 13a). A similar felsic and/or silicic source rock inference can be derived from ternary plots of Th*10-V-Ni (Bracciali et al. 2007; Fig. 13b) and bivariate plot of LREE/HREE versus Eu/Eu*(Tiwari et al. 2023; Fig. 13c). Moreover, source intermixing of granite and granodiorite, acidic, and intermediate rocks can be seen from the plots of Sc-La-Th (Jinliang and Xin 2008; Fig. 14a), Rb versus K (Shaw 1968; Fig. 14b), Sc versus Th/Sc (Schoenborn and Fedo 2011; Fig. 14c), and Zr/Sc versus Th/Sc (McLennan 1993; Fig. 14d). Based on the above whole rock geochemical characterization of the sandstones of Gondwana Group, it can be inferred that the source of sediments is predominantly from granitic/felsic/silicic rocks, although intermixing of acidic and intermediate rocks with minor inputs from mafic rocks cannot be ruled out.

5.2 Tectonic setting

The composition of sandstones derived from various source terrains is governed by plate tectonics (Dickinson and Suczek 1979). QFL (where Q is total quartz, F is total feldspar, and L is lithic fragments) and Q_mFL_t (where $Q_m$is monocrystalline quartz, F is total feldspar, and $L_t$is lithic fragments + chert) ternary discrimination plots were introduced to distinguish different terrains, namely, continental blocks, magmatic arcs, and recycled orogens. The recalculated data (Table 3), when plotted in QFL and Q_mFL_t plots (Dickinson and Suczek 1979), indicate that the studied sandstones are products of rocks within the craton interior setting (Fig. 15a and b), which is denoted as a part of continental block. The source of sediments is possibly from a stable part of the craton or shield and recycled platformal sediments (Dickinson and Suczek 1979; Dickinson 1985). Moreover, quartzose sand as indicated by major oxide discriminant functions (Roser and Korsch 1988) complements the derivation of terrigenous detritus from the interior part of the craton with low relief. This is not consistent with earlier studies, where the sediments were shown to be derived from recycled orogeny (Mahanta et al. 2020).

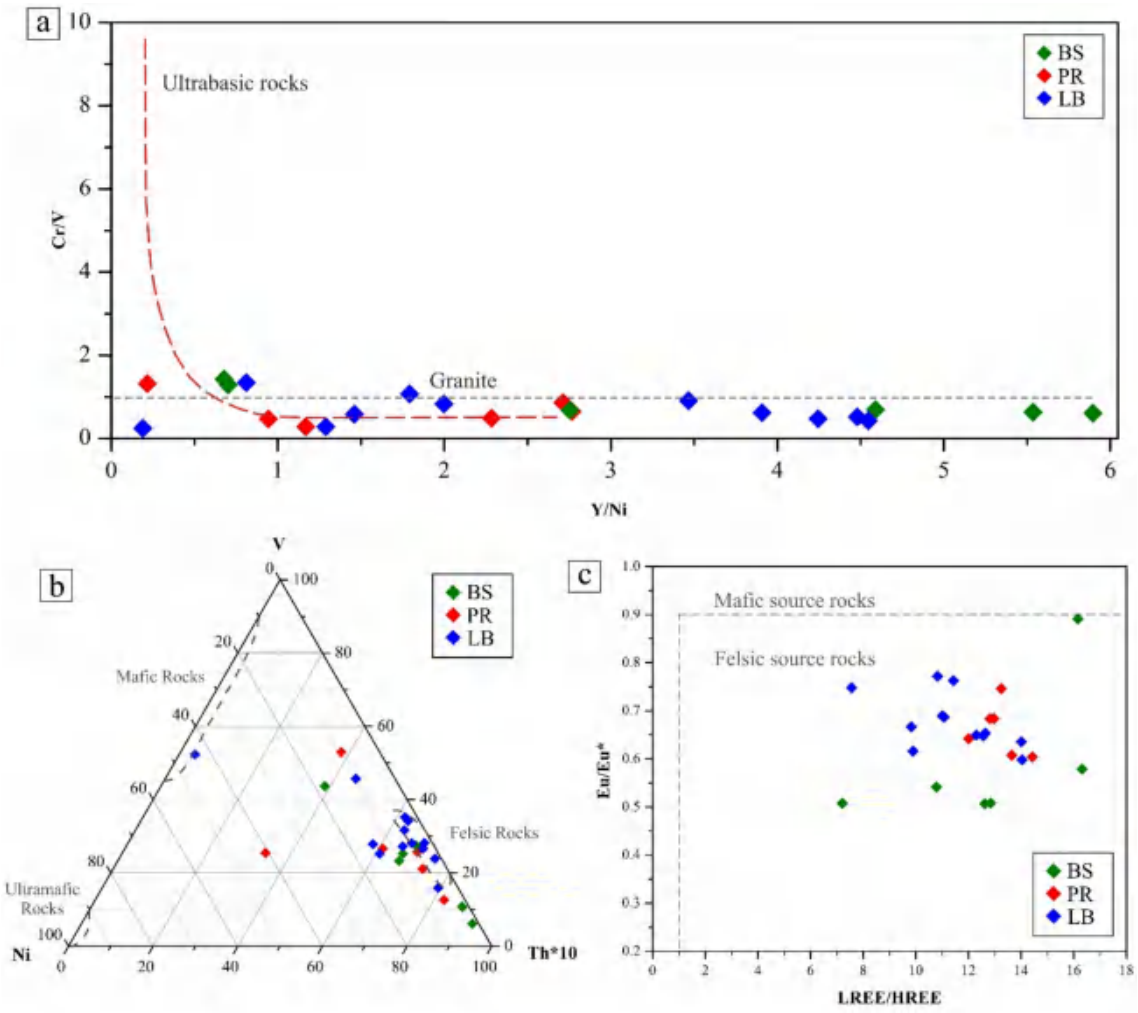

Fig. 13 Discrimination plots depicting source rocks for sandstones of the Gondwana Group: **a** bivariate plot of Y/Ni versus Cr/V (Mongelli et al. 2006), **b** ternary plot of Th*10-V-Ni (Bracciali et al. 2007); **c** bivariate plot of LREE/HREE versus Eu/Eu*(Tiwari et al. 2023)

The inferences for tectonic settings of source rocks have long been studied using geochemical characteristics of sedimentary rocks (Bhatia 1983; Bhatia and Crook 1986; Gu et al. 2002; Roser and Korsch 1988; Toulkeridis et al. 1999). Discrimination plots proposed by the above-cited researchers have been universally used in various sedimentary basins. In the present study, bivariate plots [including discriminant functions proposed by Bhatia (1983), Roser and Krosch (1988), and Gu et al. (2002)] have been used. Figure 16a indicates that the sediments were deposited predominantly in a passive margin setting, while Fig. 16b denotes the dominance of detritus originating at the active margin setting, with sediments derived from passive and arc settings as well. The above long-established plots of Bhatia (1983) and Roser and Krosch (1988) came into question because of their resulting accuracy of 0%–23% and 31.5%–52.3%, respectively, when applied to known tectonic settings of worldwide siliciclastic sediments of the Neogene-Quaternary period (Armstrong-Altrin and Verma 2005). To overcome the problem of weakness and inconsistency of traditional plots, Verma and Armstrong-Altrin (2013) proposed the use of discriminant functions, i.e., DF1(Arc-Rift-Col) m1 and DF2(Arc-Rift-Col)m2, considering high-silica [$(SiO_2)_{adj}$ = 63%–95%] and low-silica [$(SiO_2)_{adj}$ = 35%–63%] content in siliciclastic sediments for arc, rift, and collisional settings. The studied sandstones appear to cluster in both rift and collisional fields for high-silica sediments (Fig. 17a) and in rift fields for low-silica sediments (Fig. 17b). The rift field complements the passive margin setting, whereas the collision field indicates an active margin setting. Verma and Armstrong-Altrin (2016) further proposed a multidimensional discrimination diagram considering isometric log-transformed ratios (ilr) of ten major elements and a combination of ten major and trace elements (Cr, Nb, Ni, V, Y, Zr) to formulate two linear discriminant functions, $DF_{(A\text{-}P)M}$ and $DF_{(A\text{-}P)MT}$, with 87%–97% and 84%–86% success rates

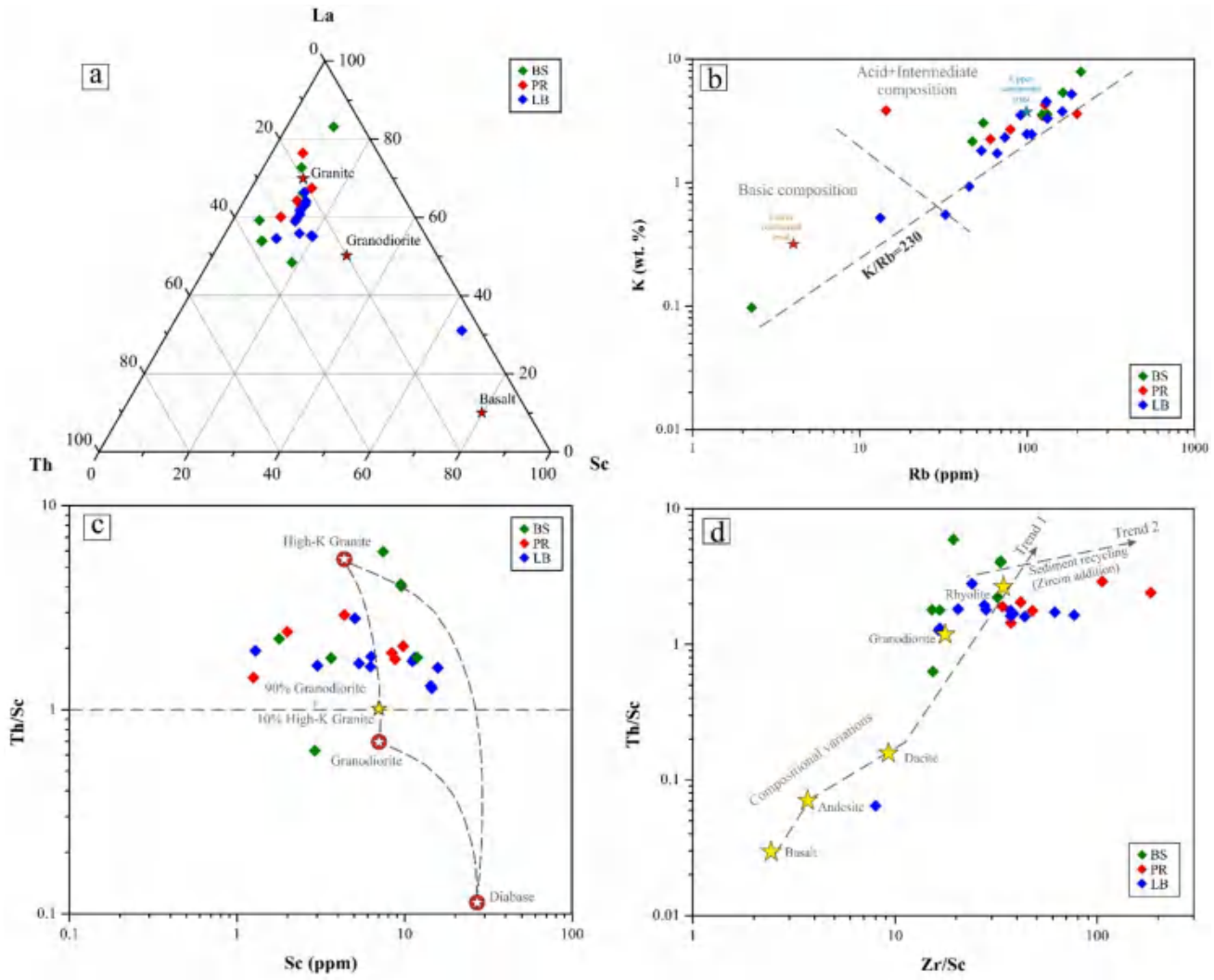

Fig. 14 **a** Ternary discrimination plot of Sc-La-Th (Jinliang and Xin 2008), **b** bivariate plot of Rb versus K (Shaw 1968), **c** bivariate plot of Sc versus Th/Sc (Schoenborn and Fedo 2011), and **d** bivariate plot of Zr/Sc versus Th/Sc (McLennan 1993) for the sandstones of the Gondwana Group

for active and passive margins, respectively, outperforming the traditional plots (0%–30%). Figure 17c and d shows the derivation of detritus from both active and passive margin tectonic settings. The only traditional diagram consistent with the new multidimensional discrimination diagram is the ternary plot of La-Th-Sc (Bhatia and Crook 1986; Fig. 18). Previous researchers did not employ the multidimensional discrimination diagram (Mahanta et al. 2020; Gogoi et al. 2021). Consequently, their conclusions do not entirely align with the findings of the current research. Their study indicates derivation of sediments predominantly from passive margin setting, although inputs from active margin and arc settings were addressed. On the other hand, the present study indicates derivations of sediments from active margin settings, which suggests that the detritus had previously been deposited within the vicinity of pre-existing active margin zones/orogenic belts (Ziegler 1992) and was later carried to the basin. The presence of well-rounded grains (Fig. 7a, b, and d) supports the possible transport of grains from a region far away from the basin of deposition, which might have been detritus of the pre-existing active margin zones. Additionally, the equal presence of sources from passive margin settings may indicate the syn-rift sedimentation process involved in rifting of the basin during the Permian period (Brookfield 1993; Biswas 1999).

5.3 Paleoclimate and source rock weathering

The proportions of framework grains of quartz, feldspar, and rock fragments are a function of changing climatic conditions (Suttner and Dutta 1986). As the climate changes, their respective proportions tend to change. Large proportions of

Table 3 Recalculated volumetric percentage of modal count of sandstones of the Gondwana Group

Sample	Quartz	Feldspar	Rock fragments	Monocrystalline quartz	Feldspar	Rock fragments + chert
	Q	F	L	Q_m	F	L_t
PR 06	95.41	3.22	1.35	95.31	3.29	1.38
PR 07	95.50	1.16	3.32	95.40	1.19	3.40
PR 7A	96.81	2.42	0.75	96.74	2.47	0.77
PR 10	82.06	13.65	4.28	81.92	13.76	4.32
PR 14	97.51	0.93	1.55	97.46	0.95	1.58
BS 01	93.06	2.06	4.86	90.02	2.97	7.00
BS 07	96.26	1.79	1.93	96.10	1.87	2.02
BS 08	97.16	1.96	0.87	97.01	2.06	0.91
BS 11	91.10	2.82	6.07	90.21	3.10	6.67
LB 07	91.39	3.58	5.01	90.36	4.01	5.62
LB 11	97.30	0.26	2.42	95.34	0.46	4.19
LB 15	97.70	0.41	1.88	97.44	0.45	2.09
LB 16	88.51	4.68	6.80	87.94	4.91	7.14
LB 19	81.20	9.02	9.77	79.50	9.83	10.65
LB 20	92.68	3.83	3.48	88.74	4.67	6.58
LB 22	95.80	1.63	2.56	95.73	1.65	2.60
LB 24A	94.75	3.96	1.28	94.16	4.40	1.43
LB 29	93.82	2.52	3.65	93.56	2.63	3.80
LB 31	97.82	1.358	0.81	97.61	1.48	0.89

**PR* Pasighat–Rengging Road section; *BS* Bomak–Sisseri Road section; *LB* Likabali–Garu–Basar Road section

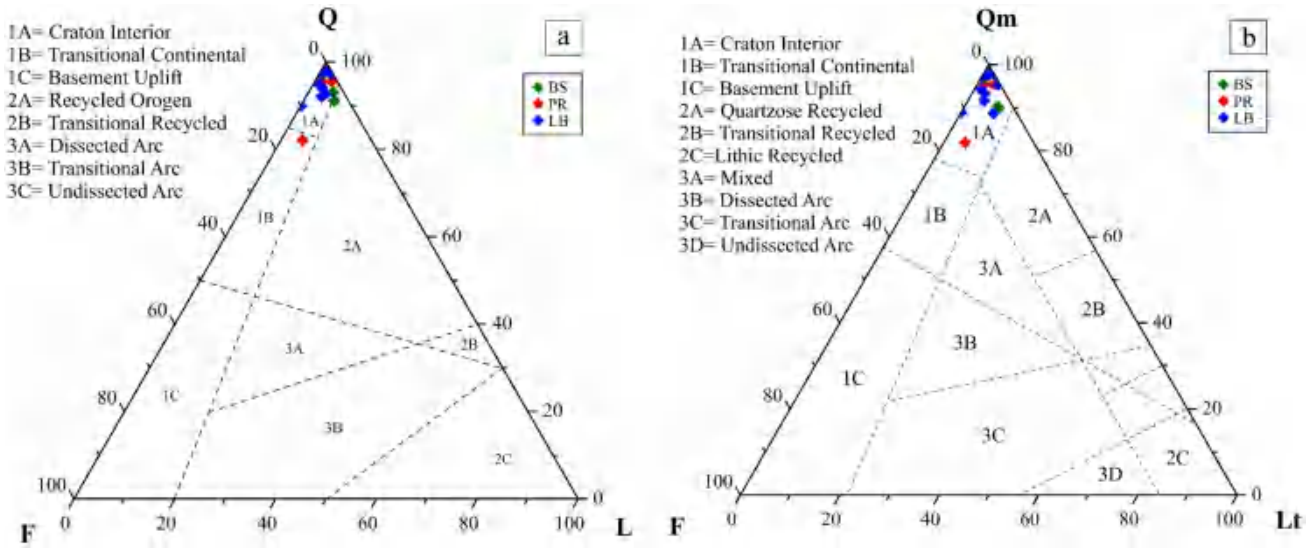

Fig. 15 **a** QFL ternary tectonic setting discrimination diagram (Dickinson and Suczek 1979) for sandstones of Gondwana Group; **b** QmFLt (Qm = monocrystalline quartz, F = feldspar; and Lt = rock fragment + chert) ternary tectonic setting discrimination diagram (Dickinson and Suczek 1979) for sandstones of the Gondwana Group

quartz with subordinate proportions of feldspar and quartz indicate humid climatic conditions (Suttner et al. 1981). Within the studied sandstones, the average percentages of quartz, feldspar, and rock fragments are 94.78%, 3.28%, and 1.93%, respectively. This indicates the prevalence of warm humid conditions, with the wettest conditions during deposition of sediments (Suttner and Dutta 1986). An alternative which is more sensitive to climate control is to focus on

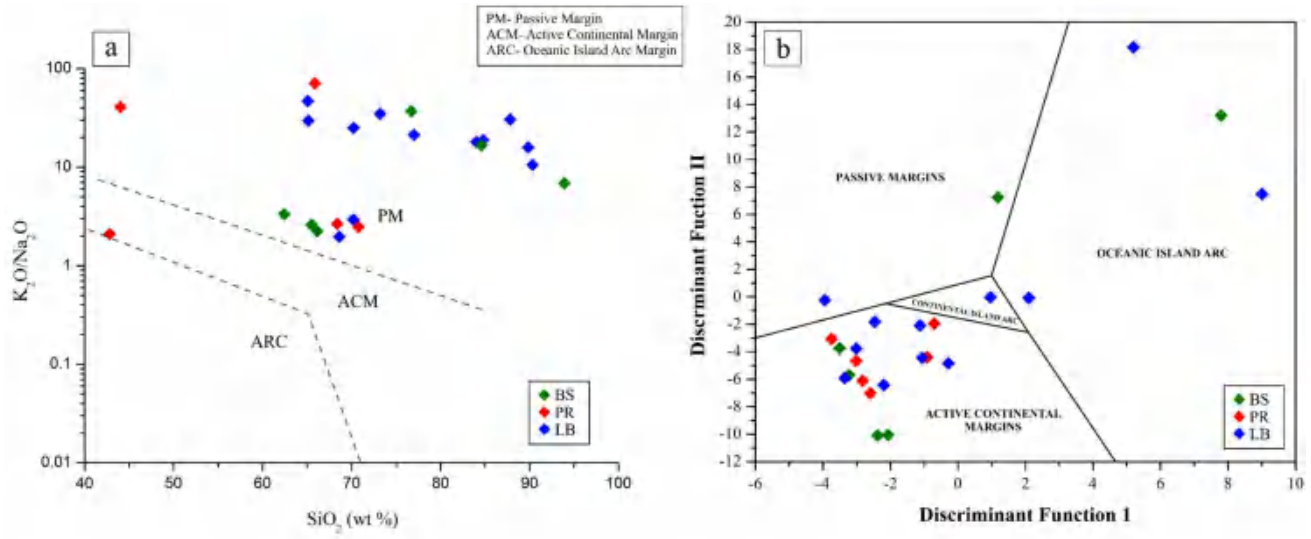

Fig. 16 **a** Bivariate tectonic discrimination diagram for sandstones of the Gondwana Group, SiO_2 versus K_2O/Na_2O (Roser and Krosch 1988); **b** tectonic discriminant plot (discriminant function I versus discriminant function II) for sandstones of the Gondwana Group (Bhatia 1983)

differences in the ratio of grain types. A log/log bivariate plot of (Q_{Total}/F + RF versus Q_p/F + RF; Suttner and Dutta 1986) when used in the studied sandstones also indicates the dominance of humid conditions, with a prevalence of semi-humid climatic conditions (Fig. 19a). A semi-quantitative weathering index [WI = C × R (WI = weathering index; C = climate; and R = relief; Grantham and Velbel 1988) coupled with a bivariate plot of ln(Q/F) versus ln(Q/R) (Weltje 1994) indicates the climate and physiography of sediments as well as the nature of the source. By considering the broad tripartite subdivision of climate and relief, the sandstones of the Gondwana Group suggest weathering indices in fields 2 and 4 (Fig. 19b), indicating sediments undergoing moderate to severe weathering. The fields also imply derivation of sediments from low plains to moderate hills in regions where humid to subhumid climatic conditions prevailed.

Geochemical elements record various changes in climate during sedimentation processes. The study of major oxides and trace elements provides a good understanding of paleoclimatic conditions (Akinlua et al. 2010; Cao et al. 2012; Galarraga et al. 2008; Ross and Bustin 2009; Roy and Roser 2013; Suttner and Dutta 1986; Vosoughi Moradi et al. 2016). The bivariate plot of $Al_2O_3 + K_2O + Na_2O$ versus SiO_2 (Suttner and Dutta 1986) separates climate into humid and arid conditions, with further subdivisions of their own. Additionally, it serves as the best representation of the chemical maturity trend as it is controlled by climatic conditions. It may be deduced from the study that a wide range of climatic conditions, from arid to humid, prevailed during the deposition of sediments, with a trend towards moderate to high chemical maturity (Fig. 19c).

Major and trace elements including Mn, Cr, Ni, V, and Co (Cao et al. 2012) are considerably enriched under wet conditions, while Ca, Mg, Sr, Ba, K, and Na are concentrated under arid conditions (Cao et al. 2012; Vosoughi Moradi et al. 2016). The relative abundance of these elements can provide insights into paleoclimate information which prevailed during the deposition of sediments. Zhao et al. (2007), Cao et al. (2012), and Moradi et al. (2016) proposed the use of the *C*-value [where C = (Fe + Mn + Cr + Ni + V + Co)/(Ca + Mg + Sr + Ba + K + Na)] as a function to show how the paleoclimate has changed over time. The calculated *C*-value (*C*-value: 0.09–1.13, avg 0.42) of the sandstones of the Gondwana Group suggests a wide range of climatic conditions ranging from arid to subarid, subhumid, and humid (Table S8; Fig. 19d). An alternative interpretation function, the paleoclimatic factor (PF) [where PF = (Fe + V + Ni + Rb + Ti)/(Ca + Mg + Sr + Ba + K + Na)] (Samad et al. 2020), uses Rb and Ti as substitutes for Mn, Cr, and Co as paleoclimate indicators. The PF of the studied sandstones ranges from 0.08 to 1.28 (avg 0.49; Table S8). When correlated with the *C*-value, it shows a significant positive linear association. Complementarily to the above elements, trace element ratios including Sr/Cu and Rb/Sr also depict climate variability. In general, the Sr/Cu ratio increases as drier conditions prevail (Bai et al. 2015; Tao et al. 2017). Values within the range of 1.3–5.0 indicate warm, humid climatic conditions, whereas ratios > 5.0 point towards hot, arid climatic conditions (Bai et al. 2015; Tao et al. 2017). Contrastingly, the Rb/Sr ratio decreases under drier conditions. Large values of Rb/Sr reflect cold conditions, and a low ratio implies warm climatic conditions (Jun et al. 1999; Xu et al. 2010). Table S8 shows that the Sr/

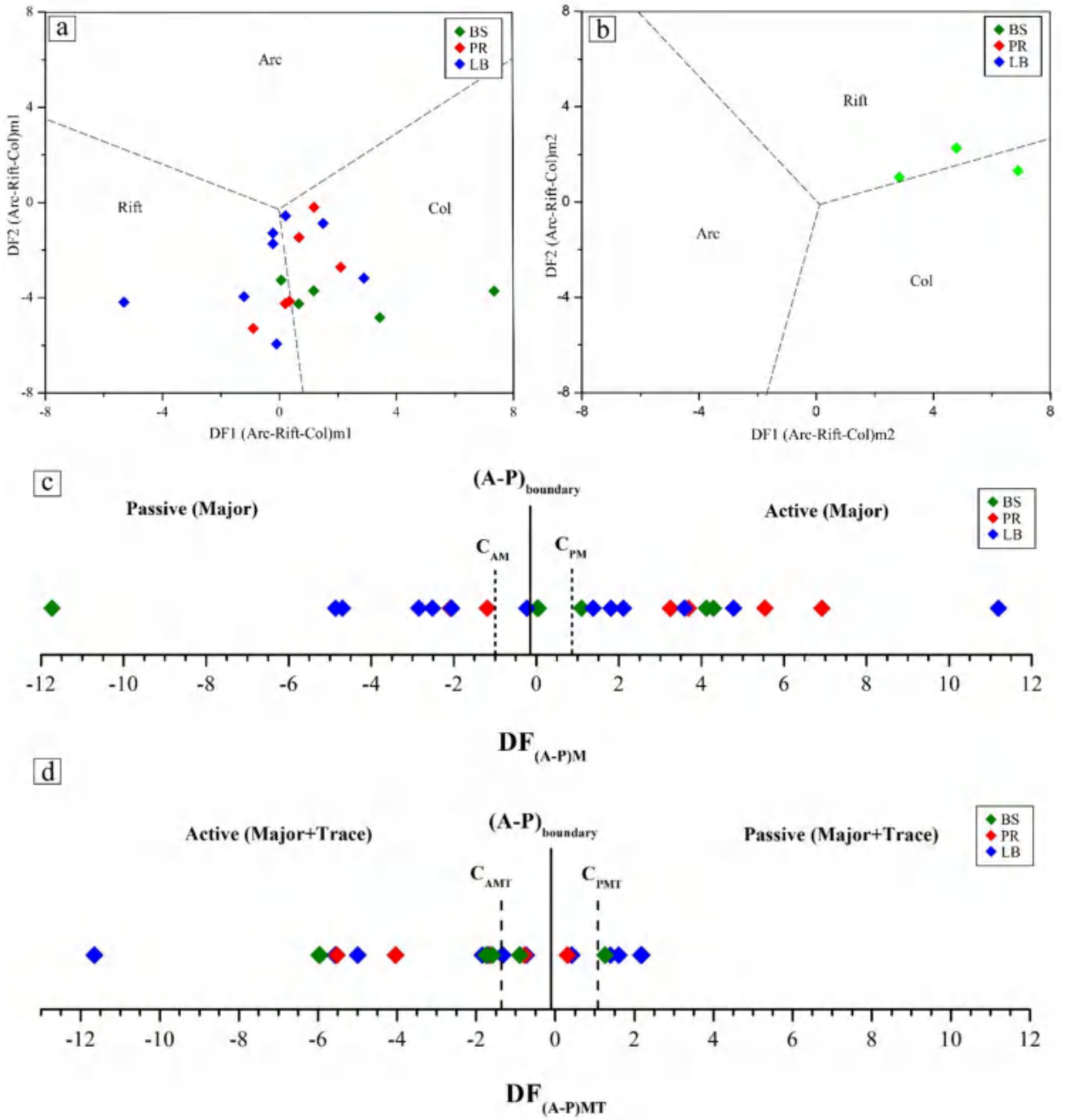

Fig. 17 **a** Multidimensional discriminant function diagram [DF1 (Arc-Rift-Col)m1 versus DF2 (Arc-Rift-Col)m1] for high-silica-content sandstones of the Gondwana Group (Verma and Armstrong-Altrin 2013). **b** Multidimensional discriminant function diagram [DF1 (Arc-Rift-Col)m2 versus DF2 (Arc-Rift-Col)m2] for low-silica-content sandstones of the Gondwana Group (Verma and Armstrong-Altrin 2013). **c** Major element-based multidimensional discriminant function diagram [DF(A-P)M] for sandstones of the Gondwana Group (Verma and Armstrong-Altrin 2016). **d** Combined major and trace element-based multidimensional discriminant function diagram [DF(A-P)MT] for sandstones of the Gondwana Group (Verma and Armstrong-Altrin 2016)

Cu ratio of the examined sandstones ranges from 0.74 to 94.34 (avg 9.04), with over 80% of the sandstones having lower ratios closer to 0.5, suggesting a prevalence of warm and humid climate conditions. The remaining 20% (higher ratios) endured significantly drier climate conditions. The Rb/Sr ratio (Table S8) supports the variations in climatic

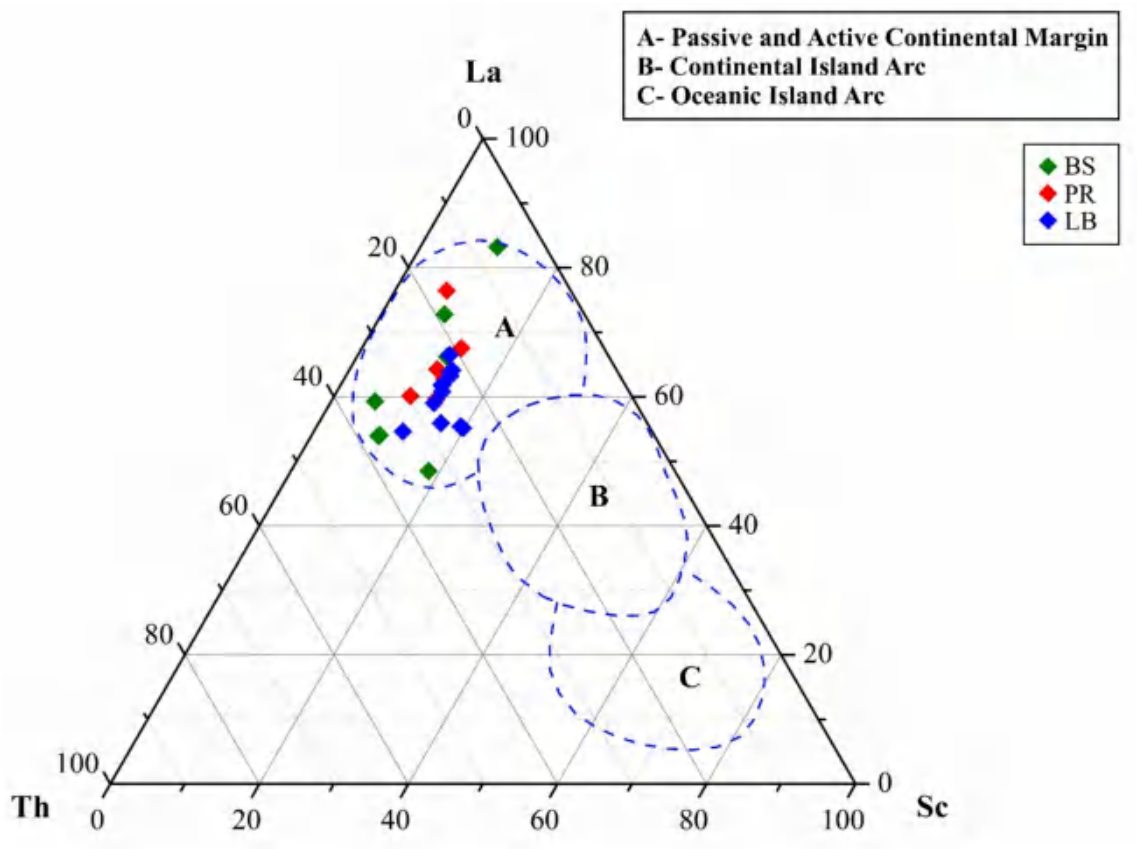

Fig. 18 Ternary plot of La-Th-Sc (Bhatia and Crook 1986) depicting the tectonic setting for the sediments of sandstones of the Gondwana Group

conditions from cold-arid to warm-humid condition as well (Rb/Sr ratio: 0.00–5.08).

By cumulative interpretation from the above paleoclimate proxies, it should be emphasized that the studied Gondwana sediments experienced a wide variety of climate conditions. This inference can be correlated to the fact that the Gondwana deposits of the Indian continental block witnessed a global climatic shift from icehouse to greenhouse conditions (Isbell et al. 2003, 2012; Fielding et al. 2008). Furthermore, separate glacial and interglacial events during the Permian period support the large variability in climate conditions (Isbell et al. 2003; Fielding et al. 2008).

Siliciclastic sediments are strongly affected by changes in mineralogy and composition due to chemical weathering at the source (Fedo et al. 1995; McLennan 1993; Nesbitt and Young 1989). Several chemical indexes have been proposed for measuring the severity of weathering (Ejeh 2021; Long et al. 2012; Nesbitt and Young 1982, 1989; Parker 1970; Potter et al. 2005). Nesbitt and Young (1982) proposed the Chemical Index of Alteration (CIA) that has been extensively used to measure the degree of weathering of rocks. CIA can be measured (using molecular proportions) as $CIA = Al_2O_3/(Al_2O_3 + CaO^* + Na_2O + K_2O) \times 100$, where CaO* denotes the quantity of CaO integrated into the sample's silicate component. It also serves as a paleoclimate indicator. More precisely, CIA values within the ranges of 50–60, 60–80, and 80–100 indicate low, moderate, and intense weathering conditions, respectively, with climates ranging from cool/arid to hot/humid conditions (Fedo et al. 1995; McLennan 1993; Nesbitt and Young 1982). The CIA can suggest source rock as well, where values for fresh basalts range from 30 to 45, for fresh granites and granodiorites range from 45 to 50, and for average shales range from 70–80 (Fedo et al. 1995; Nesbitt and Young 1982).

The CIA values of the examined sandstones range from 45.93 to 89.27 (avg 63.43; Table S8), suggesting that the sediments were subjected to low, moderate, and intense mechanical breakdown and chemical changes under circumstances ranging from cold/arid to hot/humid. Despite its frequent use to assess weathering, however, a significant drawback of the CIA is the remobilization of K during the sedimentation and metamorphic processes. Harnois (1988) proposed an alternative parameter called the chemical index of weathering (CIW) to minimize this issue. This method avoids the use of K_2O, as K content may be regarded as a diagenetic product because K-bearing minerals can be

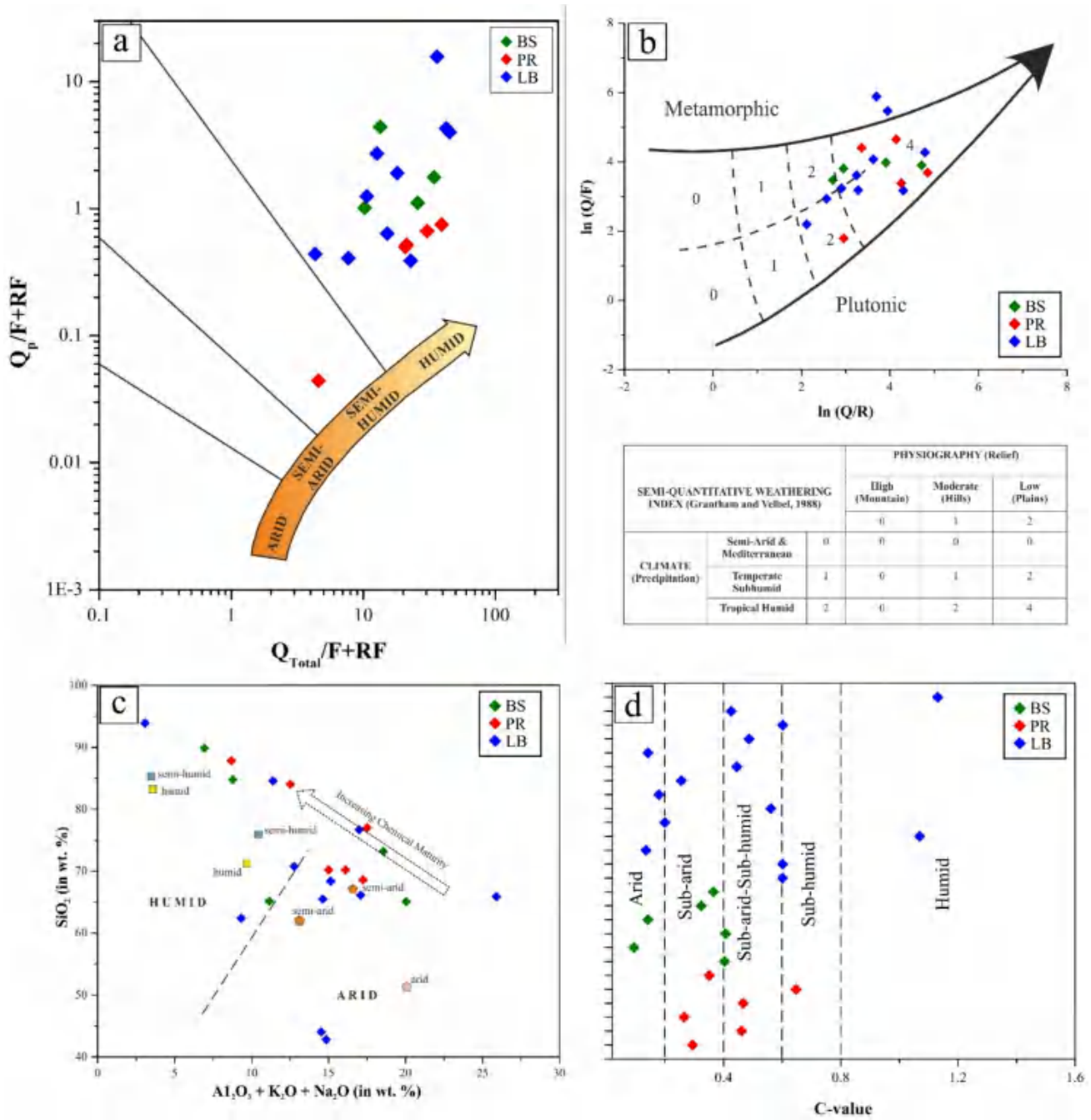

Fig. 19 **a** Log/log bivariate plot of (QTotal/F + RF) versus (Qp/F + RF) discriminating paleoclimatic conditions for sandstones of the Gondwana Group (Suttner and Dutta 1986). **b** Semi-quantitative weathering index (Weltje 1994; Grantham and Velbel 1988) showing tripartite subdivision of climate and relief for sandstones of the Gondwana Group. **c** Bivariate plot of $Al_2O_3 + K_2O + Na_2O$ against SiO_2 (Suttner and Dutta 1986) classifying paleoclimate for the sandstones of the Gondwana Group. **d** *C*-value (Zhao et al. 2007; Cao et al. 2012 and Moradi et al. 2016) as a function of paleoclimatic variations for the sandstones of the Gondwana Group

formed while entering a solution or can be adsorbed on clay minerals through ion exchange processes (Harnois 1988). CIW can be calculated (using molecular proportions) as $CIW = Al_2O_3/(Al_2O_3 + CaO^* + Na_2O) \times 100$. The CIW values of the studied sandstones range from 61.44 to 98.54 (avg 86.18; Table S8), indicating sediments derived from sources suffering moderate to intense weathering.

The extent of chemical weathering can also be estimated from the plagioclase index of alteration (PIA) (Fedo et al. 1995). This function questions the appropriateness of quantifying the intensity of chemical weathering by CIW,

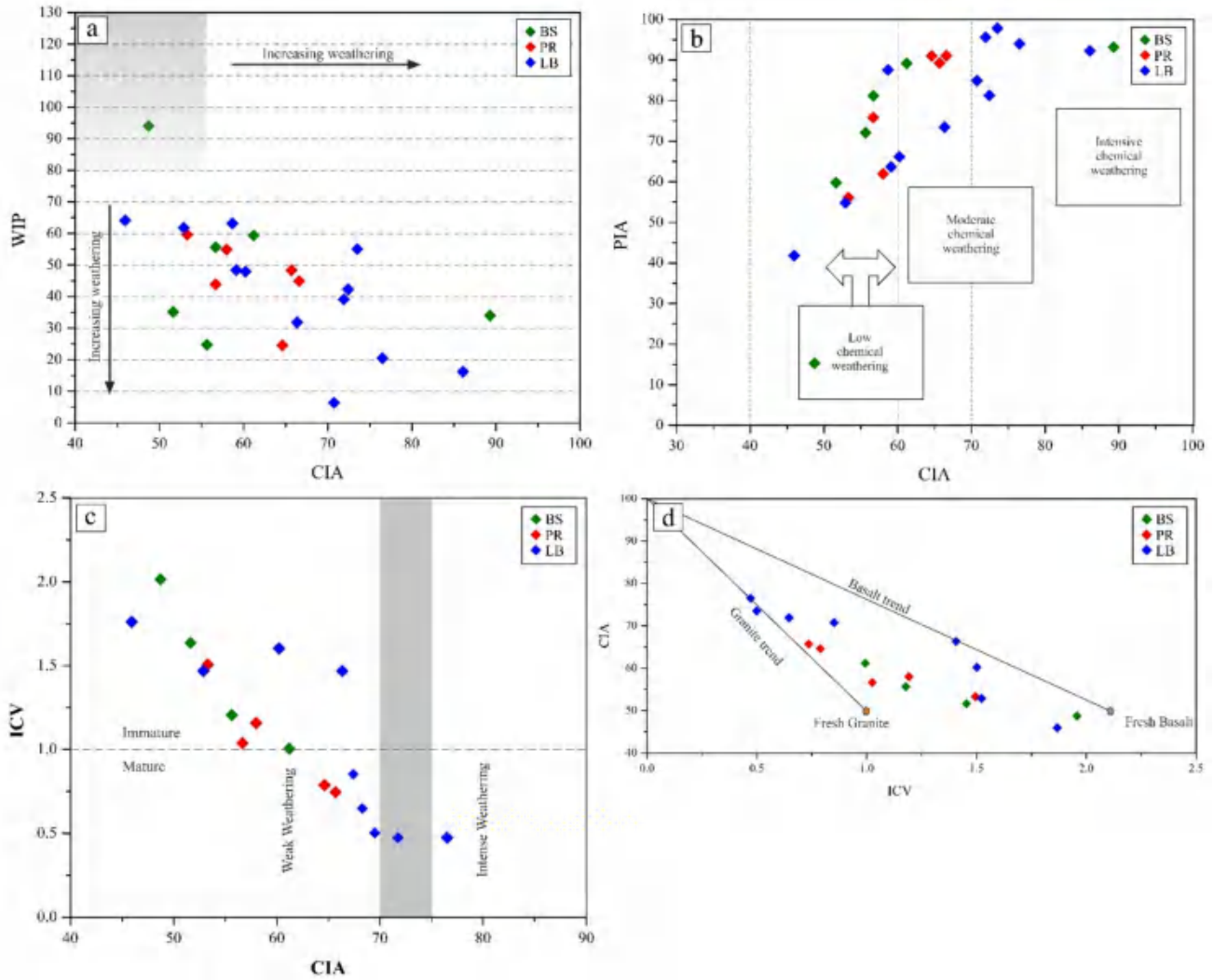

Fig. 20 **a** CIA versus WIP (Bahlburg and Dobrzinski 2011) depicting weathering intensities for source sediments of sandstones of the Gondwana Group; **b** CIA versus PIA (Ejeh 2021) depicting weathering intensities for source sediments of sandstones of the Gondwana Group; **c** CIA and ICV (Long et al. 2012) depicting sediment maturity and weathering intensities for source sediments of sandstones of the Gondwana Group; **d** ICV versus CIA (Potter et al. 2005) depicting the nature of source rock composition

where fresh potassic granite (CIW: 80) and K-feldspar (CIW: 100) show similar values for the residual products after chemical weathering (CIW of smectite: 80, CIW of kaolinite, illite and gibbsite: 100). This led to the need for monitoring of plagioclase alone, which can be accomplished through a modification of the CIA equation, as follows: $PIA = 100 \times (Al_2O_3 - K_2O)/(Al_2O_3 + CaO^* + Na_2O - K_2O)$. A PIA value of 50 implies fresh rocks, and values near 100 denote clay minerals such as kaolinite, illite, and gibbsite, which is consistent with CIA-derived values (Nesbitt et al. 1997). The PIA values of the studied sandstones range from 15.31 to 97.78 (avg 75.37; Table S8). This suggests a moderate to intense weathering of plagioclase feldspar, with a solitary sample exhibiting extremely low weathering.

Parker (1970) proposed a weathering index (WIP: Weathering Index of Parker) for silicate rocks based on alkali and alkaline earth metal proportions. The WIP reflects the changes in the proportions of Na, K, Ca, and Mg, where feldspars are transformed into clay minerals as prominent chemical weathering changes. This can be calculated as $WIP = 100 \times (2Na_2O/0.35 + MgO/0.9 + 2K_2O/0.25 + CaO^*/0.7)$. The stronger the chemical breakdown, the lower the WIP value, which is in contrast to both PIA and CIA. Generally, WIP value ranges from 0 to 100, with the least worn rocks having the highest values (Nadłonek and Bojakowska 2018). The WIP values of the studied sandstones range from 6.40 to 94.07 (avg 44.84; Table S8), indicating variability of chemical breakdown from moderate to intense weathering, while a lone sample indicates very low weathering conditions.

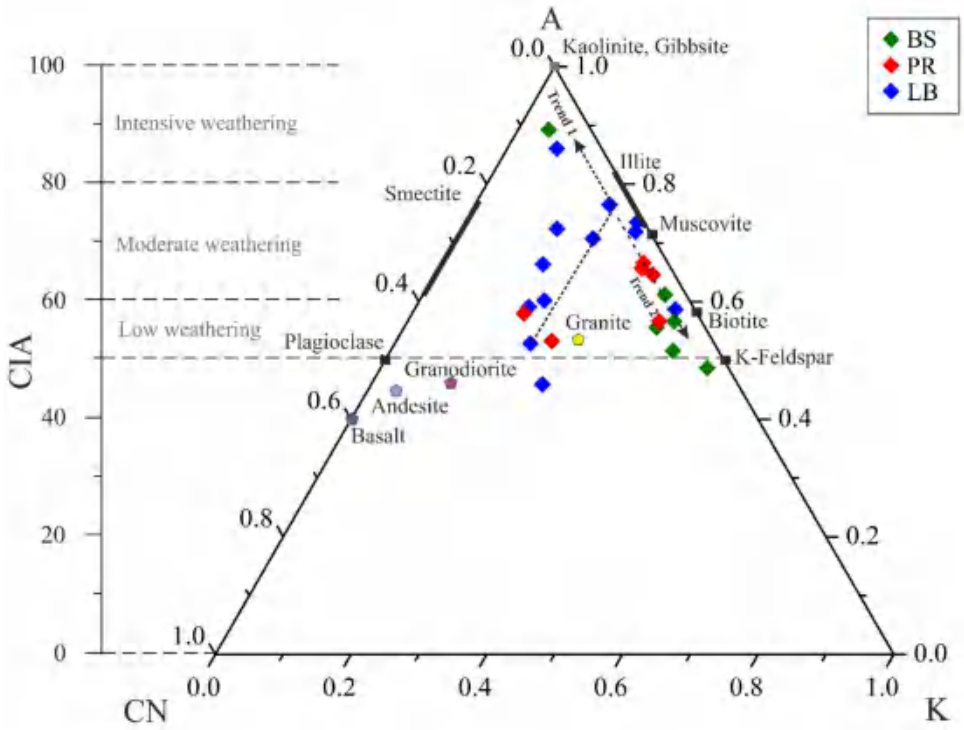

Fig. 21 A-CN-K (Nesbitt and Young 1989) ternary diagram to evaluate the composition of parent rock and weathering trend of sandstones of the Gondwana Group

The conclusions drawn from the aforementioned weathering proxies are supported by the plots that illustrate the link between CIA versus WIP (Bahlburg and Dobrzinski 2011; Fig. 20a) and CIA versus PIA (Ejeh 2021; Fig. 20b).

Cox et al. (1995) introduced the index of compositional variability [ICV = $(Fe_2O_3 + K_2O + Na_2O + CaO + MgO + MnO + TiO_2)/Al_2O_3$] to determine the maturity of source detritus of clastic sedimentary rocks. Non-clay silicate minerals possess minimal proportions of Al_2O_3 relative to clay minerals and in general show high ICV values (Cox et al. 1995). Compositionally immature clastic sedimentary rocks contain a higher proportion of non-clay silicate minerals and show a higher ICV value than mature sediments, which show low ICV values dominated by higher proportions of clay minerals (Cox et al. 1995). The studied sandstone shows a wide range of ICV values from 0.47 to 2.01 (avg 1.16; Table S8). An interrelation between CIA and ICV (Fig. 20c) (Long et al. 2012) depicts the presence of both immature (ICV > 1) and mature (ICV < 1) sediments as source, experiencing low to moderate degrees of weathering. It is worth noting that when considering the ICV values, sandstones denoting LOI% > 7 have been excluded, as the presence of high carbonate content may produce extreme ICV values (Gaschnig et al. 2016) (Table S8). Additionally, ICV serves as a predictor of source and tectonic setting. The bulk of the sediments in Fig. 20d show an intermediate composition, with inputs from juvenile granitic and basaltic rocks as a source as well (Potter et al. 2005). Compositionally immature rocks are likely to be found in active margin settings, characteristic of first-cycle deposits (Kamp and Leake 1985), while mature rocks are characteristic of cratonic environments experiencing recycling of sediments (Weaver 1989). The compositional variation trend and recycling of sediments of clastic sedimentary rocks can also be evaluated using the binary plot of Zr/Sc versus Th/Sc (McLennan 1993). Trend 1 (Fig. 14d) indicates source rock composition, while trend 2 (Fig. 14d) reveals sediment recycling processes. According to Fig. 14d, the examined sandstones are generated from acidic to intermediate igneous rocks (trend 1) as well as sources that demonstrate sediment recycling processes (trend 2), as shown by the Zr/Sc ratio. This is corroborated by enrichment and sorting of Zr (avg 266.598 ppm), which is commonly found in heavy minerals such as zircon (Basu 1976).

Nesbitt and Young (1989) proposed the A-CN-K (A: Al_2O_3; CN: $CaO^* + Na_2O$; K: K_2O) ternary diagram to evaluate the composition of parent rock and weathering trend. The horizontal line with a CIA value of 50, parallel to the CN-K axis, depicts the natural feldspar composition, also known as the feldspar join. This line serves to restrict the initial composition of source rocks (Fig. 21). The present study provides information about two trends of weathering sequences denoted as trend 1 and trend 2 (Fig. 21) within the compositional zone of A-CN-K. Trend 1 denotes a significant non-steady-state weathering process where weathering and erosion processes go hand in hand, producing sediments of varying composition over a long period (Nesbitt et al. 1997; Selvaraj and Chen 2006). This trend suggests that the

sediments were sourced primarily from fresh granitic rock with a sequential weathering trend of low, moderate, and intense chemical weathering within the compositional zone of A-CN-K. The sequence (trend 1) can be compared to an idealized state of weathering as described by Nesbitt et al. (1997). In sandstones within the low weathering region (CIA 50–60), there is an abundance of plagioclase feldspar and dearth of clay minerals. Moving into the moderate weathering region (CIA 60–80), the sandstones show an appreciable amount of feldspar along with small amounts of clay minerals such as smectite, vermiculite, and illite. As the trend approaches Al_2O_3 in the region of intense weathering (CIA 80–100), a shift in clay mineralogy occurs, favoring minerals like kaolinite and gibbsite. The non-steady-state weathering trend suggests that the region suffered tectonic activity favoring erosion associated with chemical weathering and experienced high rainfall activity in a humid region and a semi-arid region subjected to periodic storm-enhanced erosion (Nesbitt et al. 1997). Trend 2 can be regarded as the process of K-metasomatism where aluminous clay such as kaolinite may convert to illite or plagioclase may be converted to K-feldspar (along the CN-K axis) (Fedo et al. 1995). Both entail the enrichment of K_2O, which offsets the natural weathering trend. The addition of this K through the conversion of aluminous clay to illite results in decreased CIA values. However, replacing plagioclase with authigenic K-feldspar does not affect the CIA readings (Glazner 1984).

5.4 Paleoredox condition of deposition

The oxic and anoxic conditions of the paleodepositional environment can be evaluated using trace elements such as V, Cr, Ni, U, Th, Co, and Mo, as they are redox-sensitive (Yarincik et al. 2000). Authigenic U (U_{au} = total U-Th/3) is used to assess the redox condition (Wignall and Myers 1988). In general, $U_{au} > 5$ and < 5 represent sub-oxic or anoxic and oxic conditions, respectively. The values of U_{au} for the studied sandstones range from −10.34 to 0.93 (avg −3.20; Table S9), signifying the prevalence of an oxic environment. The Th/U ratio is a useful index for inferring paleoredox conditions (Wignall and Twitchett 1996). Values between 0 and 2 and between 2 and 8 indicate anoxic and strong oxidizing conditions, respectively. The Th/U ratio in the present study lies between 2.8 and 27.07 (avg 7.63; Table S9), indicating a strong oxic environment during deposition. Additionally, a converse ratio of Th/U (i.e., U/Th) proposed by Nath et al. (1997) helps in distinguishing different redox conditions, where values < 1.25 and > 1.25 represent oxic and sub-oxic/anoxic conditions, respectively. Table S9 depicts the prevalence of oxic conditions of the sandstones that range between 0.03 and 0.54 (avg 0.18). It is also possible to differentiate between oxic and anoxic conditions using the V/Cr ratio; values > 4.25, 2–4.25, and < 2 indicate sub-oxic or anoxic, dysoxic, and oxic conditions, respectively (Jones and Manning 1994). In the examined sandstones, V/Cr values lie within the range of < 2 and 2–4.25, with the majority of values < 2, indicating oxic and dysoxic conditions of deposition (Table S9). Yarincik et al. (2000) introduced the use of δU [$\delta U = U/(0.5 \times U + Th/3)$] as an index in anoxic environments, where values > 1 and < 1 indicate anoxic and oxygen-rich environments, respectively. In the present study, the examined sandstones indicate an oxygen-rich or oxic environment of deposition, with an average δU value of 0.65 (Table S9).

The Ce anomaly is widely used for evaluating redox conditions of deposition (Vosoughi Moradi et al. 2016; Cao et al. 2022). The Ce anomaly is considered to be an indicator of Ce ion exchange during stages of oxidation, which is responsive to variations in the redox environment (Wilde et al. 1996). A positive Ce anomaly (> −0.10) results where Ce is more oxidized to Ce^{4+} than its reduced form Ce^{3+}, indicating an oxic environment. In contrast, an anoxic environment will cause a negative Ce anomaly (< −0.10). The studied sandstones show an average positive Ce anomaly (0.92; Table S9), indicating a strong oxic environment.

6 Conclusions

Based on the petrographic and geochemical analyses of the sandstones of the Gondwana Group, the following conclusions regarding provenance, tectonic setting, paleoclimatic conditions of deposition, source rock paleoweathering, and paleoredox conditions of deposition can be drawn.

Petrography coupled with geochemical attributes suggests that the source for the sandstones of the Gondwana Group is predominantly granitic/felsic/acidic and/or intermediate igneous rocks, with limited inputs from metamorphic sources. The heavy minerals recorded also support the derivation of sediments from acidic to intermediate igneous rocks and low- to high-grade metamorphic rocks. Furthermore, the indication of quartzose sedimentary provenance can be linked to sediments that originated in mature continental regions. These regions may have been facilitated by sources such as highly worn granites or gneisses, or from a previous sedimentary provenance.

The sandstones of the Gondwana Group indicate that they are the products of rocks within craton interior settings, which is denoted as part of a continental block. The source of sediments is possibly from a stable part of the craton or shield and recycled platformal sediments. The sources for the sandstones were predominantly deposited in both rift and collisional settings, where the rift field complements the passive margin setting, whereas the collision field indicates an active margin setting. The derivation of sediments from

active margin settings, implies that the detritus was brought to the basin after having previously been deposited within pre-existing active margin zones or orogenic belts, whereas sources from the passive margin setting may point to the syn-rift sedimentation process that occurred during the Permian period when the basin was rifted.

The detritus of sandstones of the Gondwana Group experienced climatic conditions ranging from semi-arid/arid to semi-humid and humid conditions and suffered moderate to intense weathering conditions along with conditions of K-metasomatism. The wide variation in climate may be correlated with the shifting between glacial and interglacial events during the Permian period.

On the basis of the present study, it may be further concluded that the sandstones of the Gondwana Group were deposited under oxic conditions.

Acknowledgements The authors would like to thank the Department of Petroleum Technology, Dibrugarh University, Assam, India, for providing laboratory facilities for petrographic studies. They are also grateful to the National Geophysical Research Institute (NGRI), Hyderabad, India, for carrying out the XRF and HR-ICP-MS analysis.

Author contributions Y.K.G. prepared the main manuscript text. Y.K.G., P.B., D.B., D.B., G.K., and M.P.G. conducted the field work. Y.K.G., P.B., D.B., and D.B. did the petrographic analysis. Y.K.G., G.K., B.B., and M.P.G. carried out the interpretation from geochemical analysis. Y.K.G., G.K., and B.B. prepared the figures. All authors reviewed the manuscript.

Funding No funding was provided to the authors by any funding agencies for the present study.

Declarations

Conflict of interest The authors state that there is no conflict of interest.

References

Acharyya SK (2019) Development of gondwana basins in Indian shield. Develop Struct Geol Tecton 4:17–29. https://doi.org/10.1016/b978-0-12-815218-8.00003-0

Acharyya SK, Saha P (2008) Geological setting of the siang dome located at the eastern Himalayan Syntaxis. Himal J Sci 5(7):16–17. https://doi.org/10.3126/hjs.v5i7.1228

Akinlua A, Adekola SA, Swakamisa O, Fadipe OA, Akinyemi SA (2010) Trace element characterisation of cretaceous orange basin hydrocarbon source rocks. Appl Geochem 25(10):1587–1595. https://doi.org/10.1016/j.apgeochem.2010.08.008

André L, Deutsch S, Hertogen J (1986) Trace-element and Nd isotopes in shales as indexes of provenance and crustal growth: the early Paleozoic from the Brabant massif (Belgium). Chem Geol 57(1–2):101–115. https://doi.org/10.1016/0009-2541(86)90096-3

Armstrong Altrin JS (2009) Provenance of sands from Cazones, Acapulco, and Bahía Kino Beaches. México Rev Mex De Cienc Geológicas 26(3):764–782.

Armstrong-Altrin JS, Verma SP (2005) Critical evaluation of six tectonic setting discrimination diagrams using geochemical data of Neogene sediments from known tectonic settings. Sediment Geol 177(1–2):115–129. https://doi.org/10.1016/j.sedgeo.2005.02.004

Armstrong-Altrin JS, Lee YI, Verma SP, Ramasamy S (2004) Geochemistry of sandstones from the Upper Miocene Kudankulam Formation, southern India: implications for provenance, weathering, and tectonic setting. J Sediment Res 74(2):285–297. https://doi.org/10.1306/082803740285

Armstrong-Altrin JS, Nagarajan R, Madhavaraju J, Rosalez-Hoz L, Lee YI, Balaram V, Cruz-Martínez A, Avila-Ramírez G (2013) Geochemistry of the Jurassic and Upper Cretaceous shales from the Molango Region, Hidalgo, eastern Mexico: Implications for source-area weathering, provenance, and tectonic setting. Comptes Rendus Geosci 345(4):185–202. https://doi.org/10.1016/j.crte.2013.03.004

Bahlburg H, Dobrzinski N (2011) A review of the chemical index of alteration (CIA) and its application to the study of Neoproterozoic glacial deposits and climate transitions. Geol Soc Memoirs 36(1):81–92. https://doi.org/10.1144/m36.6

Bai YY, Liu ZJ, Sun PC, Liu R, Hu XF, Zhao HQ, Xu YB (2015) Rare earth and major element geochemistry of Eocene fine-grained sediments in oil shale- and coal-bearing layers of the Meihe Basin, Northeast China. J Asian Earth Sci 97:89–101. https://doi.org/10.1016/j.jseaes.2014.10.008

Baioumy HM (2014) Geochemistry and origin of the Cretaceous sedimentary Kaolin deposits, Red Sea. Egypt Geochem 74(2):195–203. https://doi.org/10.1016/j.chemer.2013.06.008

Banner JL, Hanson GN, Meyers WJ (1988) Rare earth element and Nd isotopic variations in regionally extensive dolomites from the Burlington–Keokuk Formation (Mississippian): Implications for REE mobility during carbonate diagenesis. SEPM J Sediment Res 58(3):415–432. https://doi.org/10.1306/212f8daa-2b24-11d7-8648000102c1865d

Baral U, Ding L, Goswami TK, Sarma M, Jan MQ, Wang C, Aminov J, Qasim M, Bezbaruah D (2021) Geochemical and geochronological studies of Abor volcanic rocks of eastern Himalaya. Geol J. https://doi.org/10.1002/gj.4268

Basu A (1976) Petrology of Holocene fluvial sand derived from plutonic source rocks: implications to paleoclimatic interpretation. SEPM J Sediment Res 46(3):694–709. https://doi.org/10.1306/212f7031-2b24-11d7-8648000102c1865d

Basu A, Young SW, Suttner LJ, James CW, Mack GH (1975) Re-evaluation of the use of undulatory extinction and polycrystallinity in detrital quartz for provenance interpretation. J Sediment Res 45(4):873–882. https://doi.org/10.1306/212f6e6f-2b24-11d7-8648000102c1865d

Basu A (1985) Influence of climate and relief on compositions of sands released at source areas. Provenance of Arenites. Springer Netherlands. pp 1–18. https://doi.org/10.1007/978-94-017-2809-6_1

Bhatia MR (1983) Plate tectonics and geochemical composition of sandstones: a discussion. J Geol 91(6):611–627. https://doi.org/10.1086/628815

Bhatia MR, Crook KAW (1986) Trace element characteristics of graywackes and tectonic setting discrimination of sedimentary basins. Contrib Mineral Petrol 92(2):181–193. https://doi.org/10.1007/BF00375292

Biswas SK (1999) A review on the evolution of rift basins in India during gondwana with special reference to Western India basins and their hydrocarbon prospects. Proc Indian Nat Sci Acad (PINSA) 65(3):261–283.

Bracciali L, Marroni M, Luca P, Sergio R (2007) Geochemistry and petrography of western tethys cretaceous sedimentary covers (Corsica and Northern Apennines): from source areas to configuration of margins. Sedimentary provenance and petrogenesis: perspectives from petrography and geochemistry. Geol Soc Am 420:73–93. https://doi.org/10.1130/2006.2420(06)

Brookfield ME (1993) The Himalayan passive margin from Precambrian to cretaceous times. Sediment Geol 84(1–4):1–35. https://doi.org/10.1016/0037-0738(93)90042-4

Burg JP, Davy P, Nievergelt P, Oberli F, Seward D, Diao ZZ, Meier M (1997) Exhumation during crustal folding in the Namche-Barwa syntaxis. Terra N 9(2):53–56. https://doi.org/10.1111/j.1365-3121.1997.tb00001.x

Cao J, Wu M, Chen Y, Hu K, Bian LZ, Wang LG, Zhang Y (2012) Trace and rare earth element geochemistry of Jurassic mudstones in the northern Qaidam Basin, northwest China. Geochemistry 72(3):245–252. https://doi.org/10.1016/j.chemer.2011.12.002

Cao C, Liu XM, Chen J (2022) Cerium anomaly as a tracer for paleo-oceanic redox conditions: a thermodynamics-based Ce oxidation modeling approach. Front Earth Sci 10:927826. https://doi.org/10.3389/feart.2022.927826

Choudhuri B, Gururajan N, Singh R (2009) Geology and structural evolution of the eastern Himalayan syntaxis. Himalayan Geol 30:17–34.

Garver JJ, Royce PR, Smick TA (1996) Chromium and nickel in shale of the taconic foreland: A case study for the provenance of fine-grained sediments with an ultramafic source. SEPM J Sediment Res Vol. 66:100-106. https://doi.org/10.1306/d42682c5-2b26-11d7-8648000102c1865d

Condie KC (1993) Chemical composition and evolution of the upper continental crust: contrasting results from surface samples and shales. Chem Geol 104(1–4):1–37. https://doi.org/10.1016/0009-2541(93)90140-E

Cox R, Lowe DR, Cullers RL (1995) The influence of sediment recycling and basement composition on evolution of mudrock chemistry in the southwestern United States. Geochim Cosmochim Acta 59(14):2919–2940. https://doi.org/10.1016/0016-7037(95)00185-9

Cullers RL (1994a) The chemical signature of source rocks in size fractions of Holocene stream sediment derived from metamorphic rocks in the Wet Mountains region, Colorado, U.S.A. Chem Geol 113(3–4):327–343. https://doi.org/10.1016/0009-2541(94)90074-4

Cullers RL (1994b) The controls on the major and trace element variation of shales, siltstones, and sandstones of Pennsylvanian-Permian age from uplifted continental blocks in Colorado to platform sediment in Kansas, USA. Geochim Cosmochim Acta 58(22):4955–4972. https://doi.org/10.1016/0016-7037(94)90224-0

Cullers RL (2000) The geochemistry of shales, siltstones and sandstones of Pennsylvanian-Permian age, Colorado, USA: implications for provenance and metamorphic studies. Lithos 51(3):181–203. https://doi.org/10.1016/S0024-4937(99)00063-8

Cullers RL, Podkovyrov VN (2002) The source and origin of terrigenous sedimentary rocks in the Mesoproterozoic Ui group, southeastern Russia. Precambrian Res 117(3–4):157–183. https://doi.org/10.1016/S0301-9268(02)00079-7

Cullers RL, Stone J (1991) Chemical and mineralogical comparison of the Pennsylvanian fountain formation, Colorado, U.S.A. (an uplifted continental block) to sedimentary rocks from other tectonic environments. Lithos 27(2):115–131. https://doi.org/10.1016/0024-4937(91)90024-F

Cullers RL, Barrett T, Carlson R, Robinson B (1987) Rare-earth element and mineralogic changes in Holocene soil and stream sediment: a case study in the wet mountains, Colorado, U.S.A. Chem Geol 63(3–4):275–297. https://doi.org/10.1016/0009-2541(87)90167-7

Cullers RL, Basu A, Suttner LJ (1988) Geochemical signature of provenance in sand-size material in soils and stream sediments near the tobacco root batholith, Montana, USA. Chem Geol 70(4):335–348. https://doi.org/10.1016/0009-2541(88)90123-4

Dickinson WR (1970) Interpreting detrital modes of graywacke and arkose. SEPM J Sediment Res 40:695–707. https://doi.org/10.1306/74d72018-2b21-11d7-8648000102c1865d

Dickinson WR (1985) Interpreting provenance relations from detrital modes of sandstones. In: Zuffa GG (ed) Provenance of Arenites. Springer Netherlands, Dordrecht, pp 333–361. https://doi.org/10.1007/978-94-017-2809-6_15

Dickinson WR, Suczek CA (1979) Plate tectonics and sandstone composition. Am Asso Petrol Geol Bull 63:2164–2182.

Dickinson WR, Beard LS, Brakenridge GR, Erjavec JL, Ferguson RC, Inman KF, Knepp RA, Lindberg FA, Ryberg PT (1983) Provenance of North American Phanerozoic sandstones in relation to tectonic setting. GSA Bull 94(2):222–235. https://doi.org/10.1130/0016-7606(1983)94%3c222:ponaps%3e2.0.co;2

Ding L, Zhong DL, Yin A, Kapp P, Harrison TM (2001) Cenozoic structural and metamorphic evolution of the eastern Himalayan syntaxis (Namche Barwa). Earth Planet Sci Lett 192(3):423–438. https://doi.org/10.1016/S0012-821X(01)00463-0

Ding L, Qasim M, Jadoon IAK, Khan MA, Xu Q, Cai FL, Wang HQ, Baral U, Yue YH (2016) The India–Asia collision in north Pakistan: insight from the U-Pb detrital zircon provenance of Cenozoic foreland basin. Earth Planet Sci Lett 455:49–61. https://doi.org/10.1016/j.epsl.2016.09.003

Ejeh OI (2021) Geochemistry of rocks (Late Cretaceous) in the Anambra Basin, SE Nigeria: insights into provenance, tectonic setting, and other Palaeo-conditions. Heliyon 7(10):e08110. https://doi.org/10.1016/j.heliyon.2021.e08110

Faure G (1986) Principles of isotope geology, 2nd edn. Wiley, New York, p 589.

Fedo CM, Wayne Nesbitt H, Young GM (1995) Unraveling the effects of potassium metasomatism in sedimentary rocks and paleosols, with implications for paleoweathering conditions and provenance. Geology 23(10):921–924. https://doi.org/10.1130/0091-7613(1995)023%3c0921:uteopm%3e2.3.co;2

Fielding CR, Frank TD, Birgenheier LP, Rygel MC, Jones AT, Roberts J (2008) Stratigraphic imprint of the late Palaeozoic ice age in eastern Australia: a record of alternating glacial and nonglacial climate regime. J Geol Soc 165(1):129–140. https://doi.org/10.1144/0016-76492007-036

Floyd P, Leveridge B (1987) Tectonic environment of the Devonian Gramscatho basin, south Cornwall: framework mode and geochemical evidence from turbiditic sandstones. J Geol Soc 144:531–542. https://doi.org/10.1144/gsjgs.144.4.0531

Floyd PA, Winchester JA, Park RG (1989) Geochemistry and tectonic setting of Lewisian clastic metasediments from the Early Proterozoic Loch Maree Group of Gairloch, NW Scotland. Precambrian Res 45(1–3):203–214. https://doi.org/10.1016/0301-9268(89)90040-5

Folk RL (1980) Petrology of sedimentary rocks. Hemphill Publishing Company, Austin, p 184.

Galarraga F, Reategui K, Martnez A, Martínez M, Llamas JF, Márquez G (2008) V/Ni ratio as a parameter in Palaeoenvironmental characterisation of nonmature medium-crude oils from several Latin American basins. J Petrol Sci Eng 61(1):9–14. https://doi.org/10.1016/j.petrol.2007.10.001

Garcia D, Fonteilles M, Moutte J (1994) Sedimentary fractionations between Al, Ti, and Zr and the genesis of strongly peraluminous granites. J Geol 102(4):411–422. https://doi.org/10.1086/629683

Gaschnig RM, Rudnick RL, McDonough WF, Kaufman AJ, Valley JW, Hu ZC, Gao S, Beck ML (2016) Compositional evolution of the upper continental crust through time, as constrained by ancient glacial diamictites. Geochim Cosmochim Acta 186:316–343. https://doi.org/10.1016/j.gca.2016.03.020

Glazner AF (1984) A short CIPW norm program. Comput Geosci 10(4):449–450. https://doi.org/10.1016/0098-3004(84)90046-3

Gogoi M, Sarmah RK, Goswami TK, Mahanta BN, Laishram R, Saikia H, Oza B (2021) Petrography, clay mineralogy and geochemistry of lower gondwana sandstones of western Arunachal Pradesh Himalayas. India J Sediment Environ 6(4):561–583. https://doi.org/10.1007/s43217-021-00070-7

Grantham JH, Velbel MA (1988) The influence of climate and topography on rock-fragment abundance in modern fluival sands of the southern Blue Ridge Mountains. North Carolina J Sediment Res 58(2):219–227. https://doi.org/10.1306/212f8d5f-2b24-11d7-8648000102c1865d

Gu XX, Liu JM, Zheng MH, Tang JX, Qi L (2002) Provenance and tectonic setting of the Proterozoic turbidites in Hunan, South China: geochemical evidence. J Sediment Res 72(3):393–407. https://doi.org/10.1306/081601720393

Haldar SK (2020) Basic mineralogy. Introduction to mineralogy and petrology. Elsevier, pp 109–143. https://doi.org/10.1016/B978-0-12-820585-3.00003-X

Harnois L (1988) The CIW index: a new chemical index of weathering. Sediment Geol 55(3–4):319–322. https://doi.org/10.1016/0037-0738(88)90137-6

Hayashi KI, Fujisawa H, Holland HD, Ohmoto H (1997) Geochemistry of ~1.9 Ga sedimentary rocks from northeastern Labrador, Canada. Geochim Cosmochim Acta 61(19):4115–4137. https://doi.org/10.1016/S0016-7037(97)00214-7

Hodges KV (2000) Tectonics of the Himalaya and southern Tibet from two perspectives. Geol Soc Am Bull 112(3):324–350. https://doi.org/10.1130/0016-7606(2000)112324:tothas%3e2.0.co;2

Isbell JL, Miller MF, Wolfe KL, Lenaker PA (2003) Timing of late Paleozoic glaciation in gondwana: was glaciation responsible for the development of northern hemisphere cyclothems? In: Chan MA, Archer AW (eds) Extreme depositional environments: Mega end members in geologic time. Geological Society of America. https://doi.org/10.1130/0-8137-2370-1.5

Isbell JL, Henry LC, Gulbranson EL, Limarino CO, Fraiser ML, Koch ZJ, Ciccioli PL, Dineen AA (2012) Glacial paradoxes during the Late Paleozoic ice age: evaluating the equilibrium line altitude as a control on glaciation. Gondwana Res 22(1):1–19. https://doi.org/10.1016/j.gr.2011.11.005

Jinliang Z, Xin Z (2008) Composition and provenance of sandstones and siltstones in Paleogene, Huimin depression, Bohai Bay basin. Eastern China J China Univ Geosci 19(3):252–270. https://doi.org/10.1016/s1002-0705(08)60044-8

Jones B, Manning DAC (1994) Comparison of geochemical indices used for the interpretation of palaeoredox conditions in ancient mudstones. Chem Geol 111(1–4):111–129. https://doi.org/10.1016/0009-2541(94)90085-x

Kesari GK (2010) Geology and mineral resources of Arunachal Pradesh; Misc. Publ., Geol Surv India. 30, 54.

Krynine PD (1946) Microscopic morphology of quartz types. Annuals of 2nd Pan-American congress of mining and geological engineers. 35–49.

Krzeszowska E (2019) Geochemistry of the Lublin Formation from the Lublin coal basin: implications for weathering intensity, Palaeoclimate and provenance. Int J Coal Geol 216:103306. https://doi.org/10.1016/j.coal.2019.103306

Long XP, Yuan C, Sun M, Xiao WJ, Wang YJ, Cai KD, Jiang YD (2012) Geochemistry and Nd isotopic composition of the Early Paleozoic flysch sequence in the Chinese Altai, Central Asia: Evidence for a northward-derived mafic source and insight into Nd model ages in accretionary orogen. Gondwana Res 22(2):554–566. https://doi.org/10.1016/j.gr.2011.04.009

Mahanta BN, Syngai BR, Sarmah RK, Goswami TK, Kumar A (2020) Geochemical signatures of lower Gondwana sandstones of eastern Arunachal Himalayas, India: implications for tectonic setting, provenance and degree of weathering. Russ J Earth Sci 20(2):1–11. https://doi.org/10.2205/2020es000698

Mange MA, Maurer HFW (1992) Heavy minerals in colour. Springer Netherlands, Dordrecht. https://doi.org/10.1007/978-94-011-2308-2

McLennan SM (1993) Weathering and global denudation. J Geol 101(2):295–303. https://doi.org/10.1086/648222

McLennan SM, Taylor SR (1991) Sedimentary rocks and crustal evolution: tectonic setting and secular trends. J Geol 99(1):1–21. https://doi.org/10.1086/629470

Mongelli G, Critelli S, Perri F, Sonnino M, Perrone V (2006) Sedimentary recycling, provenance and paleoweathering from chemistry and mineralogy of Mesozoic continental redbed mudrocks, Peloritani mountains, southern Italy. Geochem J 40(2):197–209. https://doi.org/10.2343/geochemj.40.197

Moradi AV, Sarı A, Akkaya P (2016) Geochemistry of the Miocene oil shale (Hançili Formation) in the Çankırı-Çorum Basin, Central Turkey: Implications for Paleoclimate conditions, source–area weathering, provenance and tectonic setting. Sed Geol 341:289–303

Morton AC (1985) Heavy minerals in provenance studies. In: Zuffa GG (ed) Provenance of Arenites. Springer Netherlands, Dordrecht, pp 249–277. https://doi.org/10.1007/978-94-017-2809-6_12

Mudoi NM, Gogoi B, Dehingia P (2022) Provenance, tectonic setting, paleoweathering and paleoclimatic conditions of early to mid-Eocene sandstones of the Dalbuing Formation, Arunachal Pradesh, NE India: inferences from petrography and geochemistry. Phys Chem Earth Parts a/b/c 127:103196. https://doi.org/10.1016/j.pce.2022.103196

Mukhopadhyay G, Mukhopadhyay SK, Roychowdhury M, Parui PK (2010) Stratigraphic correlation between different Gondwana basins of India. J Geol Soc Ind 76(3):251–266. https://doi.org/10.1007/s12594-010-0097-6

Nadłonek W, Bojakowska I (2018) Variability of chemical weathering indices in modern sediments of the Vistula and Odra rivers (Poland). Appl Ecol Environ Res 16(3):2453–2473.

Nagarajan R, Madhavaraju J, Nagendra R, Armstrong-Altrin JS, Moutte J (2007) Geochemistry of Neoproterozoic shales of the Rabanpalli Formation, Bhima Basin, Northern Karnataka, southern India: Implications for provenance and paleoredox conditions. Revista Mexicana De Ciencias Geologicas 24(2):150–160.

Nagender Nath B, Bau M, Ramalingeswara Rao B, Rao CM (1997) Trace and rare earth elemental variation in Arabian Sea sediments through a transect across the oxygen minimum zone. Geochim Cosmochim Acta 61(12):2375–2388. https://doi.org/10.1016/s0016-7037(97)00094-x

Najman Y, Bickle M, BouDagher-Fadel M, Carter A, Garzanti E, Paul M, Wijbrans J, Willett E, Oliver G, Parrish R, Akhter SH, Allen R, Ando S, Chisty E, Reisberg L, Vezzoli G (2008) The Paleogene record of Himalayan erosion: Bengal basin. Bangladesh Earth Planet Sci Lett 273(1–2):1–14. https://doi.org/10.1016/j.epsl.2008.04.028

Nesbitt HW, Young GM (1982) Early Proterozoic climates and plate motions inferred from major element chemistry of lutites. Nature 299:715–717. https://doi.org/10.1038/299715a0

Nesbitt HW, Young GM (1989) Formation and diagenesis of weathering profiles. J Geol 97(2):129–147. https://doi.org/10.1086/629290

Nesbitt HW, Fedo CM, Young GM (1997) Quartz and feldspar stability, steady and non-steady-state weathering, and petrogenesis of siliciclastic sands and muds. J Geol 105(2):173–191. https://doi.org/10.1086/515908

Palmer DA, Wesolowski DJ (1992) Aluminum speciation and equilibria in aqueous solution: II. The solubility of gibbsite in acidic sodium chloride solutions from 30 to 70°C. Geochim Cosmochim Acta 56(3):1093–1111. https://doi.org/10.1016/0016-7037(92)90048-N

Parker A (1970) An index of weathering for silicate rocks. Geol Mag 107(6):501–504. https://doi.org/10.1017/S0016756800058581

Phillips OA, Falana AO, Adebayo AJ (2017) The geochemical composition of sediment as a proxy of provenance and weathering intensity: a case study of southwest Nigeria's Coastal creeks. Geol Geoph Environ 43(3):229. https://doi.org/10.7494/geol.2017.43.3.229

Potter PE, Barry Maynard J, Depetris PJ (2005) Mud and mudstones: introduction and overview. Springer, Berlin, Heidelberg. https://doi.org/10.1007/b138571

Priya RK, Tewari VC, Ranjan RK (2019) Permian Tethyan transgression in Sikkim-Darjeeling Himalaya with special reference to the Paleoclimatic event. Bull Nepal Geol Soc 36:233–240.

Roser BP, Korsch RJ (1986) Determination of tectonic setting of sandstone-mudstone suites using SiO_2 content and K_2O/Na_2O ratio. J Geol 94(5):635–650. https://doi.org/10.1086/629071

Roser BP, Korsch RJ (1988) Provenance signatures of sandstone-mudstone suites determined using discriminant function analysis of major-element data. Chem Geol 67(1–2):119–139. https://doi.org/10.1016/0009-2541(88)90010-1

Ross DJK, Bustin RM (2009) Investigating the use of sedimentary geochemical proxies for paleoenvironment interpretation of thermally mature organic-rich strata: examples from the Devonian-Mississippian shales. Western Can Sediment Basin Chem Geol 260(1–2):1–19. https://doi.org/10.1016/j.chemgeo.2008.10.027

Roy DK, Roser BP (2013) Climatic control on the composition of Carboniferous-Permian Gondwana sediments, Khalaspir basin. Bangladesh Gondwana Res 23(3):1163–1171. https://doi.org/10.1016/j.gr.2012.07.006

Samad SK, Mishra DK, Mathews RP, Ghosh S, Mendhe VA, Varma AK (2020) Geochemical attributes for source rock and Palaeoclimatic reconstruction of the Auranga Basin. India J Petrol Sci Eng 185:106665. https://doi.org/10.1016/j.petrol.2019.106665

Sarma M, Bezbaruah D, Goswami TK, Baral U (2020) Geologic and tectonic evolution of the Yinkiong Group and Abor volcanic rocks in the eastern Himalaya: an overview of geologic data. Geotectonics 54(3):395–409. https://doi.org/10.1134/S0016852120030097

Schoenborn WA, Fedo CM (2011) Provenance and paleoweathering reconstruction of the Neoproterozoic Johnnie Formation, southeastern California. Chem Geol 285(1–4):231–255. https://doi.org/10.1016/j.chemgeo.2011.04.014

Selvaraj K, Chen CTA (2006) Moderate chemical weathering of subtropical Taiwan: constraints from solid-phase geochemistry of sediments and sedimentary rocks. J Geol 114(1):101–116. https://doi.org/10.1086/498102

Sengupta SM (1994) Introduction to sedimentology. 1st edn. CRC Press.

Shaw DM (1968) A review of K-Rb fractionation trends by covariance analysis. Geochim Cosmochim Acta 32(6):573–601. https://doi.org/10.1016/0016-7037(68)90050-1

Singh S (1993) Geology and tectonics of the eastern syntaxial bend. Arunachal Himalaya J Himalayan Geol 4(2):149–163.

Singh AK, Bikramaditya Singh RK (2012) Petrogenetic evolution of the felsic and mafic volcanic suite in the Siang window of Eastern Himalaya. Northeast India Geosci Front 3(5):613–634. https://doi.org/10.1016/j.gsf.2012.01.004

Suttner LJ, Dutta PK (1986) Alluvial sandstone composition and paleoclimate, framework mineralogy. J Sediment Petrol 56(3):329–345. https://doi.org/10.1306/212F8909-2B24-11D7-8648000102C1865D

Suttner LJ, Basu A, Mack GH (1981) Climate and the origin of quartz arenites. SEPM J Sediment Res 51(4):1235–1246. https://doi.org/10.1306/212f7e73-2b24-11d7-8648000102c1865d

Tao S, Xu YB, Tang DZ, Xu H, Li S, Chen SD, Liu WB, Cui Y, Gou MF (2017) Geochemistry of the Shitoumei oil shale in the Santanghu Basin, northwest China: Implications for paleoclimate conditions, weathering, provenance and tectonic setting. Int J Coal Geol 184:42–56. https://doi.org/10.1016/j.coal.2017.11.007

Taylor SR, McLennan SM (1985) The continental crust: Its composition and evolution. Blackwell, USA, p 349.

Tiwari B, Ghosh S, Kumar S, Varma AK (2023) Trace and rare earth elements in the Permian shales: geochemical paradigms. Arab J Geosci 16(4):1–22. https://doi.org/10.1007/s12517-023-11361-w

Tortosa A, Palomares M, Arribas J (1991) Quartz grain types in Holocene deposits from the Spanish central system: some problems in provenance analysis. Geol Soc Lond Spec Publ 57(1):47–54. https://doi.org/10.1144/gsl.sp.1991.057.01.05

Toulkeridis T, Clauer N, Kröner A, Reimer T, Todt W (1999) Characterization, provenance, and tectonic setting of fig tree greywackes from the Archaean Barberton Greenstone Belt, South Africa. Sediment Geol 124(1–4):113–129.

Valdiya KS (1997) Himalaya, the northern frontier of east Gondwanaland. Gondwana Res 1(1):3–9. https://doi.org/10.1016/S1342-937X(05)70002-2

Van de Kamp PC, Leake BE (1985) Petrography and geochemistry of feldspathic and mafic sediments of the northeastern Pacific margin. Earth Env Sci Trans Roy Soc Edinb 76(4):411–449. https://doi.org/10.1017/s0263593300010646

Venkatachala BS, Tiwari RS (1987) Lower Gondwana marine incursions: periods and pathways. J Palaeosciences 36:24–29. https://doi.org/10.54991/jop.1987.1556

Verma SP, Armstrong-Altrin JS (2013) New multi-dimensional diagrams for tectonic discrimination of siliciclastic sediments and their application to Precambrian basins. Chem Geol 355:117–133. https://doi.org/10.1016/j.chemgeo.2013.07.014

Verma SP, Armstrong-Altrin JS (2016) Geochemical discrimination of siliciclastic sediments from active and passive margin settings. Sediment Geol 332:1–12. https://doi.org/10.1016/j.sedgeo.2015.11.011

Wadia DN (1931) Syntaxis of the NW Himalayas: Its rocks, tectonics and orogeny. Records Geol Survey India 65(2):189–220.

Wang W, Cawood PA, Pandit MK (2021) India in the Nuna to Gondwana supercontinent cycles: clues from the north Indian and Marwar blocks. Am J Sci 321(1–2):83–117. https://doi.org/10.2475/01.2021.02

Weaver CE (1989) Clays, muds, and shales. Development in Sedimentology. Elsevier, Amsterdam. 44:1–5.

Weltje GJ (1994) Provenance and dispersal of sand-sized sediments: Reconstruction of dispersal patterns and sources of sand-sized sediments by means of inverse modelling techniques. Geologica Ultraiectina. 121.

Wignall PB, Myers KJ (1988) Interpreting benthic oxygen levels in mudrocks: a new approach. Geology 16(5):452. https://doi.org/10.1130/0091-7613(1988)016%3c0452:ibolim%3e2.3.co;2

Wignall PB, Twitchett RJ (1996) Oceanic anoxia and the end Permian mass extinction. Science 272(5265):1155–1158. https://doi.org/10.1126/science.272.5265.1155

Wilde P, Quinby-Hunt MS, Erdtmann BD (1996) The whole-rock cerium anomaly: a potential indicator of eustatic sea-level changes in shales of the anoxic facies. Sediment Geol 101(1–2):43–53. https://doi.org/10.1016/0037-0738(95)00020-8

Wopfner H, Jin XC (2009) Pangea Megasequences of tethyan gondwana-margin reflect global changes of climate and tectonism in Late Palaeozoic and Early Triassic times: a review. Palaeoworld 18(2–3):169–192. https://doi.org/10.1016/j.palwor.2009.04.007

Worash G, Valera R (2002) Rare earth element geochemistry of the Antalo Supersequence in the Mekele Outlierr (Tigray region, northern Ethiopia). Chem Geol 182(2–4):395–407. https://doi.org/10.1016/S0009-2541(01)00328-X

Xu H, Liu B, Wu F (2010) Spatial and temporal variations of Rb/Sr ratios of the bulk surface sediments in Lake Qinghai. Geochem Trans 11:3. https://doi.org/10.1186/1467-4866-11-3

Yarincik KM, Murray RW, Lyons TW, Peterson LC, Haug GH (2000) Oxygenation history of bottom waters in the Cariaco Basin, Venezuela, over the past 578,000 years: results from redox-sensitive metals (Mo, V, Mn, and Fe). Paleoceanography 15(6):593–604. https://doi.org/10.1029/1999pa000401

Yin A (2006) Cenozoic tectonic evolution of the Himalayan orogen as constrained by along-strike variation of structural geometry, exhumation history, and foreland sedimentation. Earth Sci Rev 76(1–2):1–131. https://doi.org/10.1016/j.earscirev.2005.05.004

Zhao ZY, Zhao JH, Wang HJ, Liao JD, Liu CM (2007) Distribution characteristics and applications of trace elements in Junggar Basin. Nat Gas Explor Develop 30(2):30–32.

Ziegler PA (1992) Geodynamics of rifting and implications for hydrocarbon habitat. Tectonophysics 215(1–2):221–253. https://doi.org/10.1016/0040-1951(92)90083-I

Zimmermann U, Bahlburg H (2003) Provenance analysis and tectonic setting of the Ordovician clastic deposits in the southern Puna Basin. NW Argentina Sedimentol 50(6):1079–1104. https://doi.org/10.1046/j.1365-3091.2003.00595.x